Nanoneedle-Based Materials for Intracellular Studies

Julia E. Sero and Molly M. Stevens

Abstract

Nanoneedles, defined as high aspect ratio structures with tip diameters of 5 to approximately 500 nm, are uniquely able to interface with the interior of living cells. Their nanoscale dimensions mean that they are able to penetrate the plasma membrane with minimal disruption of normal cellular functions, allowing researchers to probe the intracellular space and deliver or extract material from individual cells. In the last decade, a variety of strategies have been developed using nanoneedles, either singly or as arrays, to investigate the biology of cancer cells in vitro and in vivo. These include hollow nanoneedles for soluble probe delivery, nanocapillaries for single-cell biopsy, nano-AFM for direct physical measurements of cytosolic proteins, and a wide range of fluorescent and electrochemical nanosensors for analyte detection. Nanofabrication has improved to the point that nanobiosensors can detect individual vesicles inside the cytoplasm, delineate tumor margins based on intracellular enzyme activity, and measure changes in cell metabolism almost in real time. While most of these applications are currently in the proof-of-concept stage, nanoneedle technology is poised to offer cancer biologists a powerful new set of tools for probing cells with unprecedented spatial and temporal resolution.

Keywords

Nanoneedles · Nanopipettes · Nanocapillaries · Nanoelectrodes · Nanostraws · Nanowires · Nanobiopsy · Nanoparticles · Intracellular sensing · Reactive oxygen species (ROS) · Redox probes · Scanning ion conductance microscopy (SICM) · Fluid force microscopy · Molecular beacons · Surface-enhanced Raman scattering (SERS) · Cancer biomarker · Cell metabolism · Mitochondria · Intracellular pH · Dual carbon electrodes (DCE) · Cytoskeleton

J. E. Sero
Biology and Biochemistry Department, University of Bath, Claverton Down, Bath, UK

M. M. Stevens (✉)
Institute for Biomedical Engineering, Imperial College London, London, UK
e-mail: m.stevens@imperial.ac.uk

Abbreviations

AFM	Atomic force microscopy
ANE	Asymmetric nanopore electrodes
ATP	Adenosine triphosphate
BNS	Branched nanostraws
CNT	Carbon nanotube
CTC	Circulating tumor cell
CTSB	Cathepsin B
DCE	Dual carbon electrodes
ELISA	Enzyme-linked immunosorbent assay
FET	Field-effect transistor
FIB	Focused ion beam
FRET	Forster resonance energy transfer
GFP	Green fluorescent protein
IP	Immunoprecipitation
iPSC	Induced pluripotent stem cells
LPS	Lysophosphatidic acid
MB	Methylene blue
MEA	Multielectrode array
MFP	Microfluidic probe
MMP	Matrix metalloproteinase
MnSOD	Manganese superoxide dismutase
MS	Mass spectroscopy
NES	Nano-electrospray
NFP	Nanofountain probe
Osbpy	Osmium bipyridine
PEG	Polyethylene glycol
qPCR	Quantitative polymerase chain reaction
RCA	Rolling circle amplification

F. Fontana, H. A. Santos (eds.), *Bio-Nanomedicine for Cancer Therapy*, Advances in Experimental Medicine and Biology 1295, https://doi.org/10.1007/978-3-030-58174-9_9

RFP	Red fluorescent protein
RNS	Reactive nitrogen species
ROS	Reactive oxygen species
SCIM	Scanning ion conductance microscopy
SECM	Scanning electrochemical microscopy
SEM	Scanning electron microscope
SERS	Surface-enhanced Raman scattering
SOD	Superoxide dismutase
SWCNT	Single-walled carbon nanotube

The 2010s witnessed a "Cambrian explosion" in the fabrication of nanoscale materials. Nanoneedles have emerged as a core technology for probing living cells due to their ability to interface directly with the cytoplasm and cause minimal disruption to normal cellular functions. Here we use the term "nanoneedles" as a catch-all term for high aspect ratio nanostructures, meaning materials with tip diameters of less than ~500 nm and 1–10 microns in length (Fig. 1a). High aspect ratio nanostructures have been fabricated from a variety of materials, from inorganic semiconductors to metals to carbon (Fig. 1b–f). The nanoneedle literature has a varied and often inconsistent nomenclature, including nanowires, nanospears, nanocapillaries, nanostraws, nanopipettes, nanotubes, nanopillars, nanoelectrodes, and more. Nanoneedles can be solid structures, such as porous Si pillars [1] and filled nanoelectrodes [2], or hollow tubes, such as alumina nanostraws [3], quartz nanopipettes [4], and double-barreled nanopipettes. They may be used as single probes for individual cells or as arrays that can interact with cellular populations. Nanoneedles can be used to deliver cargos, remove cellular contents, or measure electrochemical signals – or even all of these at once. Many excellent recent reviews have explored the larger theme of nanoneedles and nanoscale sensors in cell biology [5–9]. In this chapter, we will focus on advances in the use of nanoneedles for intracellular biosensing over the last decade and on how these technologies have been, or could be, applied to cancer research.

1 Types of Nanoneedles Used for Intracellular Sensing

Nanoneedles that directly access the intracellular space can be classified as solid or hollow structures and as single-cell probes or multicell arrays. Solid nanoneedles have been fabricated by a combination of microfabrication techniques, such as wet and dry etching of silicon wafers. These approaches can be tailored to produce nanopillars with well-defined geometries which can be sharpened into conical tips. The processing used to shape nanoneedles can also be used to alter their material properties. For example, wet etching can be used to form solid nanoneedles of mesoporous silicon. Such nanoneedle arrays have been used to deliver cargos, such as nucleic acids, and as carriers of biological probes [10, 11]. Alternatively, nanowires composed of silicon and other inorganic semiconductor materials can be grown on substrates by the vapor-liquid-solid mechanism to produce vertical arrays [12]. Atomic force microscopy (AFM) tips may be sharpened to nanoscale points that can penetrate cell membranes [13]. Hollow nanoneedles include nanostraw arrays, nanopipettes or nanocapillaries, carbon nanotubes, and AFM tips with micro- or nanochannels. Nanostraw arrays are fabricated by coating porous polycarbonate membranes with metals and then etching the support to reveal nanometer-diameter tubes [14]. Fluid force microscopy combines sharpened AFM tips with micro- or even nanofluidic channels [15–17]. Probes such as nanoendoscopes made from carbon nanotubes benefit from being cylindrical, rather than conical or pyramidal, with well-defined radii of 50–200 nm that have less potential to damage cells [18]. Nanoelectrodes can be fabricated in many ways to form either solid or hollow probes. For example, filled nanoelectrodes may be pulled around a conductive material such as Pt wire, filled with Pt black, or flame-etched to expose a nanoscale carbon fiber tip [19, 20]. Hollow nanocapillary electrodes provide multifunctionality, as they can deliver or extract material as well as measure electrochemical signals [21]. Moreover, electrochemical signals can be used to guide probes into position as well as detect analytes [22–24].

Methods for intracellular sensing can be broadly subdivided into direct in situ interfacing with the cytosol, delivery of bioprobes, and extraction of cellular contents. Direct interfacing strategies include insertion of nanoelectrodes, nanoneedle-bound optical or electrochemical sensors, and antibody-functionalized nanoneedles that bind to cytoplasmic proteins. Nanoneedle-mediated delivery can be used to load cells with membrane impermeant chemicals or materials. Cellular contents can be extracted with single nanocapillaries or by using arrays of nanostraws or nanoneedles. Many of these strategies overlap and most can be multiplexed. Readouts for intracellular sensing can be optical (generally fluorescent), mechanical, and/or electrical. Electrical sensors are multifunctional, as they can measure changes in conductance that denote cell penetration, the presence of cell-generated reactive oxygen species (ROS) that are involved in cell metabolism, and the production of ROS such as hydrogen peroxide from enzymatic reactions.

2 The Cell-Nanoneedle Interface

The size of nanoneedles means that they are uniquely able to interact with biological structures on the cellular scale. For example, caveolae are membrane invaginations involved in endocytosis that are similar in size to the smaller end of nanoneedle tips in use today, typically 60–80 nm in diameter

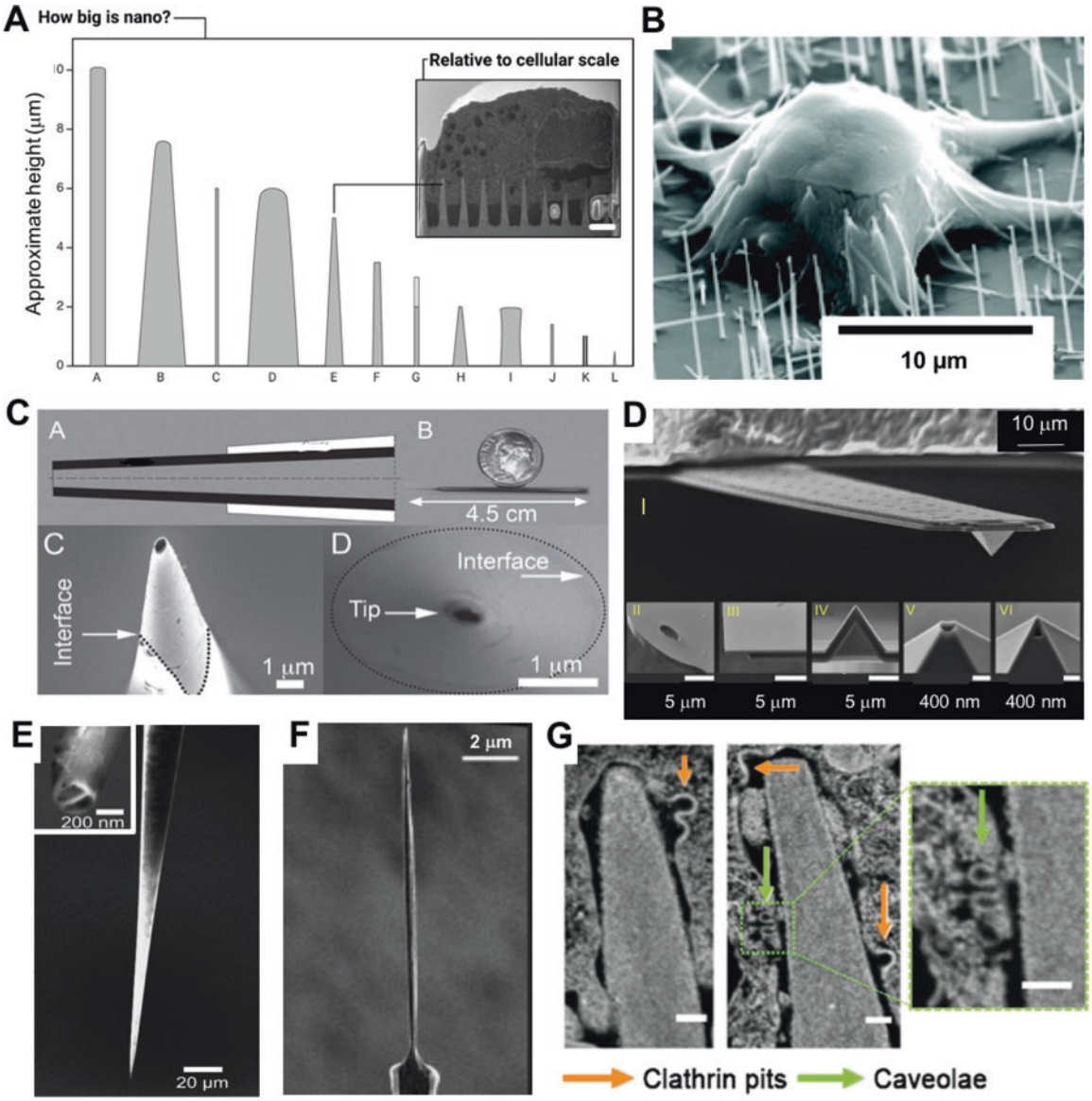

Fig. 1 (**a**) Nanoneedle scales relative to one another and the cellular scale. Scale bar in inset = 2 μm. Nanostructures depicted: (A) Si pillar, (B) diamond nanoneedle, (C) Si nanowire, (D) Plasmonic micropillar, (E) Porous Si nanoneedle, (F) hollow Si nanowire, (G) nanoelectrode, (H) diamond nanoneedle, (I) Si micropillar, (J) quartz nanopillar, (K) hollow nanostraw, (L) carbon fiber nanoelectrode tip. (Reproduced with permission from [9]. Copyright 2020, Wiley). (**b**) SEM of cell adhering to silicon nanowires. (Adapted with permission from [179]. Copyright 2007, American Chemical Society). (**c**) Carbon nanopipettes. (I) Schematic of nanopipette cross section. (II) Photograph of a carbon nanopipette fabricated from a pulled capillary. (III) SEM side view of carbon nanopipette tip. (IV) SEM axial view of a 200 nm carbon nanopipette tip. Dotted lines indicate the quartz-carbon interface. (Reproduced with permission from [2]. Copyright 2014, IOP Publishing). (**d**) SEM images of microchanneled cantilevers for fluidic force microscopy (FluidFM). (I) Perspective view of cantilever with pyramidal tip. (II) Zoomed-in image of the aperture of a tipless probe. (III–IV) Zoomed-in images of the microchannel and hollow pyramid after FIB sectioning. (V) Zoomed-in image of lithographically obtained 300 nm aperture in correspondence with pyramidal apex. (VI) Zoomed-in image of FIB-drilled triangular 300 nm aperture. (Reproduced with permission from [16]. Copyright 2014, Elsevier). (**e**) SEM image of spearhead field-effect transistor dual carbon electrode. Inset: cross section of tip after FIB milling. (Adapted with permission from [109]. Copyright 2016, American Chemical Society). (**f**) SEM of the tip of a conical carbon fiber nanoelectrode used for intracellular vesicle electrochemical cytometry. (Adapted with permission from [125]. Copyright 2015, Wiley). (**g**) FIB-SEM image of engulfed nanoneedle showing two classes of endocytic vesicles, clathrin-coated pits (orange arrows) and caveolae (green arrows). Scale bars = 100 nm. (Adapted with permission from [28]. Copyright 2019, The Authors)

[25, 26]. Caveolae and clathrin pits are clearly visible around mesoporous Si nanoneedles by focused ion beam-scanning electron microscopy (FIB-SEM), in which thin sections of cellular material are milled away and consecutive SEM images are acquired (Fig. 1g) [27, 28]. Furthermore, extracellular matrix components such as collagen fibrils in tissues are on the order of 10–300 nm [29, 30], which is in the mid-range of nanoneedle tips used for intracellular studies. Thus,

distortions of the plasma membrane and underlying cytoskeleton induced by nanoneedles are in the realm of sizes that cells have evolved to experience. However, the extent of cytosolic interaction with different kinds of nanostructures and the circumstances under which membrane penetration occurs are contingent upon a number of factors. The interface between cells and nanoneedles remains an open area of investigation, and many questions remain to be answered about how or when membrane penetration occurs.

In order for nanoneedles to access the cytoplasm, they must breach the plasma membrane and underlying cortical cytoskeleton as well as any extracellular barriers, such as the glycocalyx. When cells settle on nanoneedles by gravity, the plasma membrane has time to adapt to the nanotopography and deform around the nanostructures [31, 32]. Nanoneedles may be thus be engulfed, their cargo may be endocytosed, and/or the cell membrane may be ruptured and resealed around the obstruction (Fig. 2a). Spontaneous penetration is rare in the absence of membrane disruption by applied forces (micromanipulation or hypergravity) or electroporation [33–39]. Chemical modifications such as phospholipids [40] or hydrophobic molecules [41, 42] can also enhance membrane penetration. Current evidence suggests that in addition to the interfacing force between nanoneedle and cell membrane, the key factors for penetration are membrane fluidity, speed of insertion, and tip sharpness [43, 44] (Fig. 2b). The sharpness of the nanoneedle tip is also critical for cell viability, as under some circumstances, tips greater than 400 nm in diameter begin to compromise cellular function [45]. Current in silico models of the cell membrane-nanoneedle interface indicate that these effects are also highly dependent on other geometric parameters, such as the relative spacing between nanoneedles [31, 46]. The architecture of the cortical cytoskeleton and the composition of the plasma membrane play important roles in determining whether nanoneedles can access the cytoplasm [34, 36, 37]. Cancer cells show characteristic changes in stiffness and membrane fluidity [47–49] that may complicate nanoneedle-based experiments but could also be useful as diagnostic metrics [27]. For in-depth discussions of the mechanics of membrane penetration by nanoneedles, see [5, 9].

Electrical conductance is a well-established tool for detecting cellular contact and cell penetration. Changes in ionic current at the probe tip indicate when cell penetration has occurred [2, 50] (Fig. 3a, c, d). Nanoneedle probes are often integrated with scanning ion conductance microscopy (SICM) to precisely control their position and detect cell membrane penetration. SICM works by measuring the increase in resistance in a micro- or nanopipette probe as it approaches a nonconductive or poorly conductive surface.

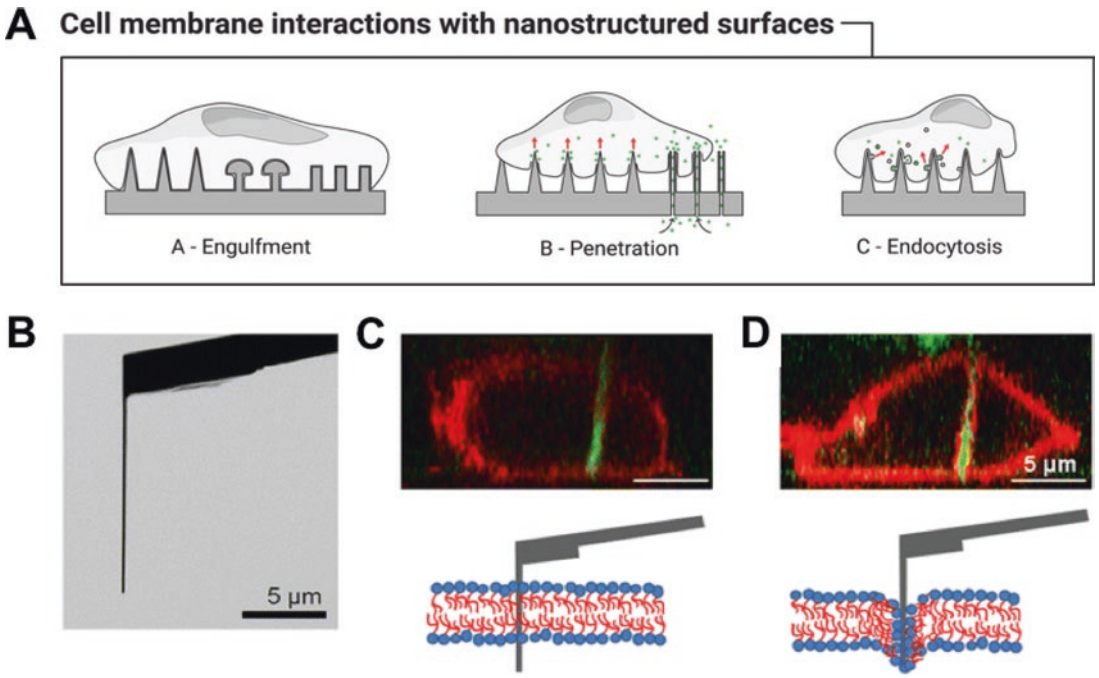

Fig. 2 Nanoneedle-cell interactions. (**a**) Cell membrane interactions on nanoneedle arrays. Cells can engulf nanostructures and spontaneous penetration is rare unless additional membrane rupture is induced, e.g., by electroporation. Endocytosis is enhanced around nanoneedles. (Reproduced with permission from [9]. Copyright 2020, Wiley). (**b–d**) Cell penetration by AFM-operated nanoneedles depends on membrane fluidity, insertion speed, temperature, surface chemistry, and cell stiffness. (**b**) Scanning ion microscopy image of AFM cantilever nanoneedle. (**c**) Side view confocal microscopy images and schematics of nanoneedle (green) insertion through the plasma membrane (red). (**d**) Unsuccessful insertion shown by red signal from the membrane surrounding the nanoneedle. (Reproduced under Creative Commons license from [44])

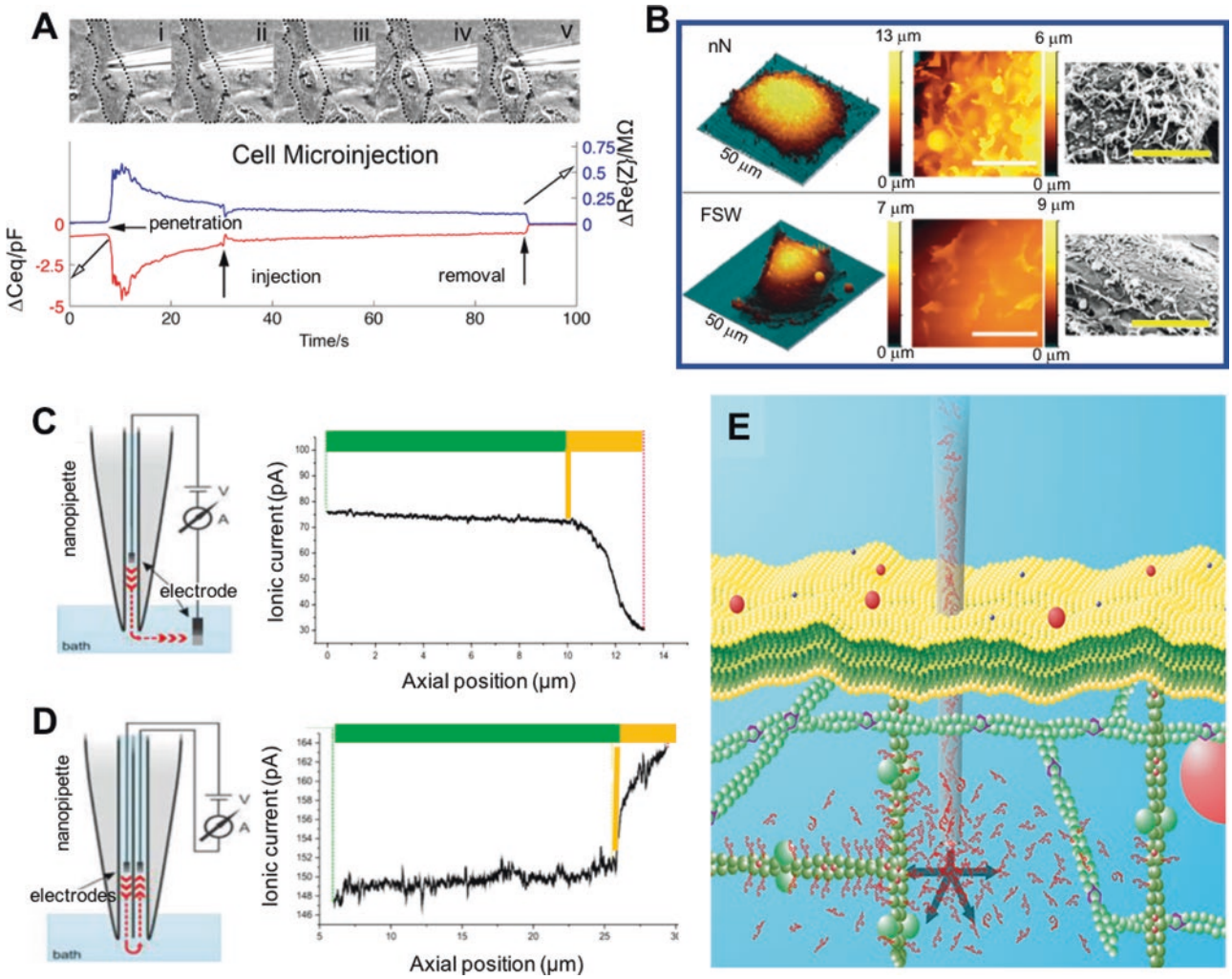

Fig. 3 Hollow nanoelectrodes used for cell surface mapping, detection of membrane penetration, and delivery of biomolecular probes. (**a**) Penetration and microinjection using carbon nanopipettes. Top: micrographs of carbon nanocapillary interfaced with a cell (dotted line) over time. Bottom: changes in capacitance (red) and resistance (blue) over time during cell penetration, injection, and probe removal. (Adapted with permission from [2]. Copyright 2014, IOP Publishing). (**b**) Topographical mapping of the cell surface by scanning ion conductance microscopy (SICM). Increased membrane ruffling was observed on the apical surface of cells seeded on arrays of mesoporous silicon nanoneedles (nN) compared to cells seeded on flat Si wafer (FSW). Left: 3D topographical SICM maps. Middle: 2D SICM scan (10 μm × 10 μm). Right: SEM images of apical membranes. Scale bars = 5 μm. (Adapted with permission from [28]. Copyright 2019, The Authors). (**c**) Single-barreled nanopipette and approach curve. The nanopipette is initially positioned ~20 μm above the cell. The counter electrode is placed in the culture medium and the initial voltage is set to ±60 mV, leading to an ionic current of 70–100 pA. As the tip approaches the cell (green bar) and penetrates the plasma membrane (yellow line), the ionic current decreases sharply (yellow bar). (**d**) Double-barreled nanopipette and approach curve. During the approach, applying positive voltage between electrodes leads to a weak ionic current (green bar). Upon penetrating the cell (yellow line), the ionic current increases (yellow bar). (**e**) Schematic of nanoinjection. Single living cells can be specifically labeled by injecting probes using a nanopipette with tip diameter ~100 nm. Once inside the cell, increasing or reversing the voltage leads to diffusion of the molecules out of the cell by electrophoresis. (Reproduced with permission from [59]. Copyright 2015, American Chemical Society)

This method is commonly used as a noncontact method for mapping cell surface topography [22, 23, 51]. For example, Gopal et al. used SICM to show that seeding human mesenchymal stem cells on nanoneedle arrays led to increased formation of membrane ruffles on the apical surface [28] (Fig. 3b). Electrical conductance measurement can thus be combined with intracellular cargo delivery or sampling using hollow nanocapillaries.

3 Delivery of Molecular Probes to Monitor Cellular Processes

Nanoneedle-based strategies can efficiently introduce a wide range of unbound probes directly into the cytosol, including cell-impermeant molecules, and can even deliver cocktails of cargos for multistep reactions and multiplexed sensing. Intracellular probes label cellular components and

are used to monitor biological processes based on electrochemical or fluorescent readouts. Over the last decade, many methods to deliver molecular and nanoparticle probes directly into cells have been developed using nanoneedles [52], nanowires [53], carbon nanotubes [54], nanopipettes [55, 56], nanofluidic devices [15, 57], and nanoelectrodes [58]. Hennig et al. used electrophoretic nanoinjection of fluorescent probes to label DNA, actin, microtubules, and organelles in living cells with signal-to-noise ratios that enabled rapid super-resolution imaging (dSTORM) [59] (Fig. 3e). They showed that nanoneedle tip diameter was an important factor in determining cell viability following electrophoresis, and best results were obtained using nanopipettes with tip diameters of 100 nm or less [45]. Espinosa and colleagues developed "nanofountain probes" (NFP), nanocapillaries fabricated from etched AFM tips with sub-100 nm resolution that act like fountain pens delivering ink through capillary action, to inject cells with fluorescent-labeled nanodiamonds [57] and nucleic acids [60] (Fig. 4a). They found that applying an electrical pulse enhanced NFP cargo delivery without compromising cell viability [61]. They used this localized electroporation system to deliver DNA- and RNA-based molecular beacons that detect specific mRNAs (GAPDH) in live HeLa cells [62]. Molecular beacons are nucleotide hairpins that contain a fluorophore at one end and a quencher at the other; when hybridized to the target, the resulting spatial separation of the 5′ and 3′ ends produces a change in the fluorescent signal [63] (Fig. 4b).

Abnormal protein glycosylation drives cancer cell signaling, adhesion, migration, and stem cell maintenance, and many cell surface tumor markers are glycoproteins [64]. Hollow nanocapillaries called nanostraws are an effective way to deliver cell-impermeable probes [3, 65, 66] (Fig. 5a–d). To fabricate these arrays, nanoporous track-etched polycarbonate membranes are coated with metal (Al, Au, or Pt) by a conformal technique such as atomic-layer deposition, and then the membrane is etched on one side to expose protruding nanostraws. Nanostraws used for cell interfacing experiments are on the order of 100 nm in diameter and 1 μm in height depending on the etch time. The spacing of the nanostraws depends on the

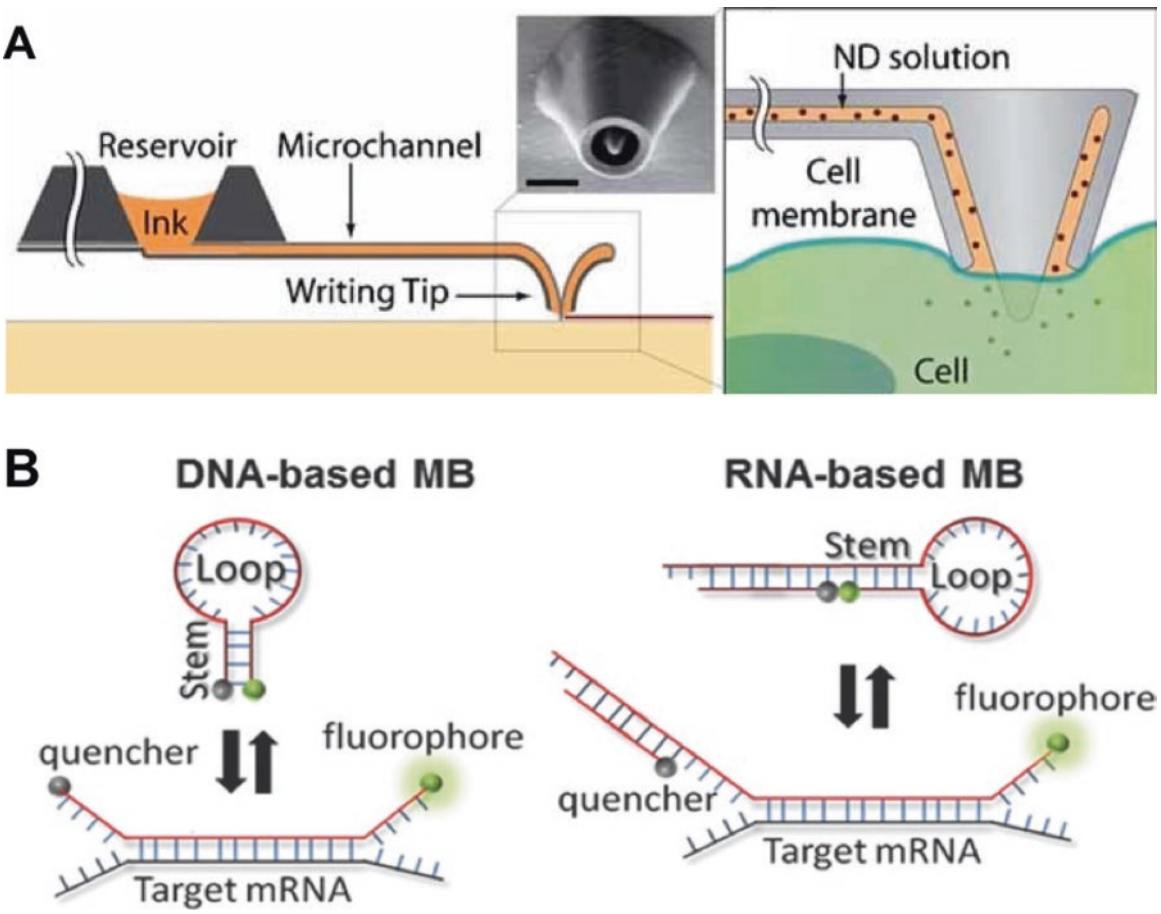

Fig. 4 Nanofountain probe-mediated delivery of fluorescent molecular beacons. (**a**) Schematic of nanofountain probe AFM tip for cell injection. (Copyright (2015) Wiley. Used with permission from [57]). (**b**) Schematic of DNA- and RNA-based molecular beacons (MB) used to detect GAPDH mRNA in live cells. (Copyright (2009) Wiley. Adapted with permission from [62])

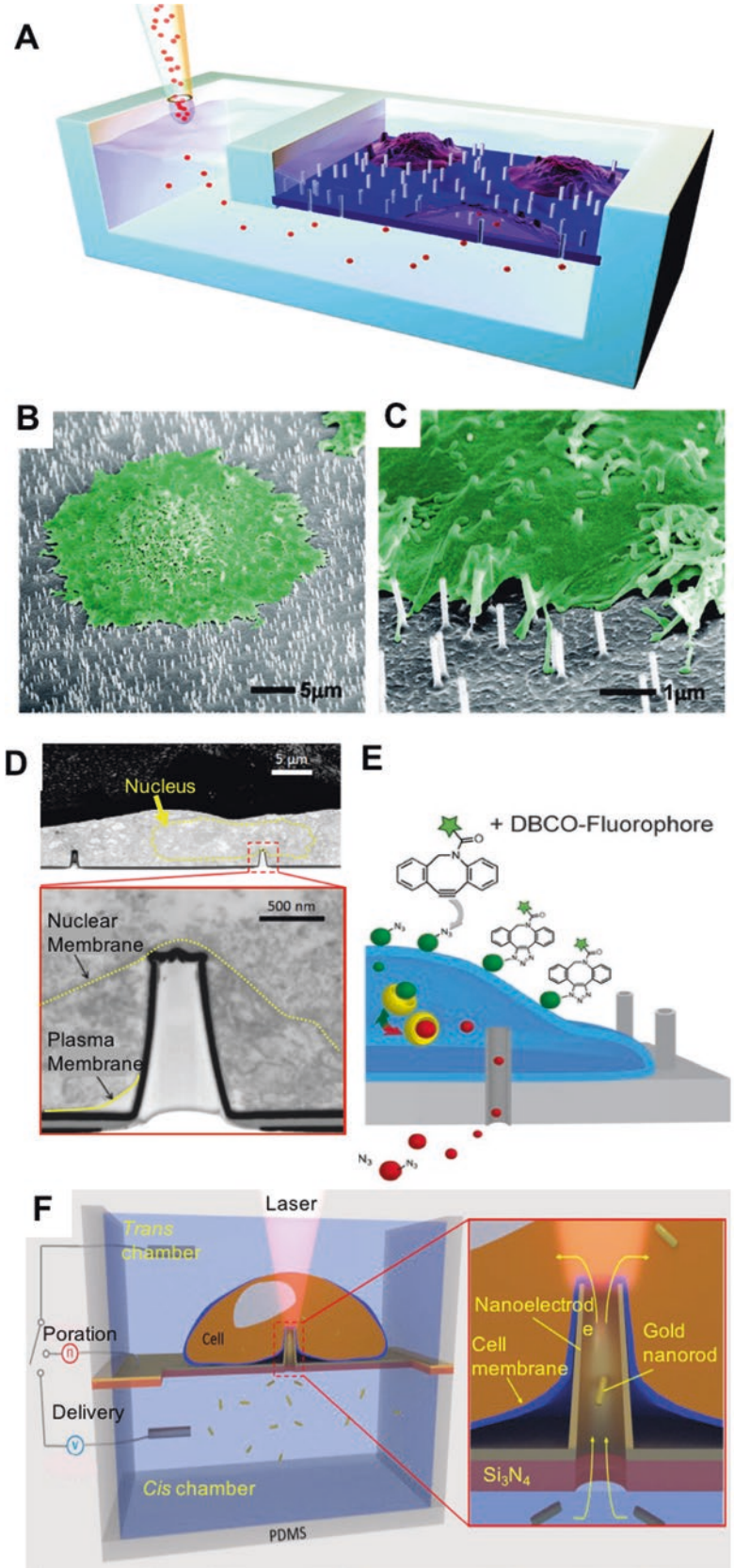

Fig. 5 Nanostraw arrays for cargo delivery and extraction. (**a**) Schematic of nanostraw microfluidic system, cross section (not to scale). (**b**, **c**) SEM images of cells (green) cultured on 100-nm-diameter nanostraws at a density of 10^8 nanostraws/cm^2. (**d**) Top: cross-sectional SEM image of a cell cultured on nanostraw electrodes. Bottom: magnified image of inset showing cell membrane wrapped around the hollow nanostraw and impingement of the nuclear envelope (dashed line). (**e**) Schematic of nanostraw-mediated delivery of azido sugars, which are converted into sialic acid groups and incorporated into cell surface glycoproteins. The azide moiety is then labeled with a fluorophore-conjugated probe (DBCO). (**f**) Schematic of 3D hollow nanoelectrode device for gold nanorod delivery. Electroporation is induced by pulsed voltage. Nanorods are delivered from the lower to the upper chamber through nanostraws due to a direct current potential between two Pt wire electrodes. A laser beam excites the Raman signals of the gold nanorods inside the cell. (**a**–**c** reproduced with permission from [3]. Copyright 2011, American Chemical Society. **d** and **f** adapted with permission from [83], https://pubs.acs.org/doi/10.1021/acs.nanolett.8b03764. Copyright 2019, American Chemical Society. **e** adapted with permission from [67]. Copyright 2017, Wiley)

porosity of the polycarbonate membrane or ion beam milling parameters. Nanostraw-bearing membranes are overlaid onto microfluidic channels, and cells are seeded in the upper chamber. Agent delivery, or cellular contents extraction, is controlled from the lower channel. Spontaneous contact between the nanostraw interior and cytosol is rare when cells adhere to nanostraw arrays because the plasma membrane has time to engulf the nanostructures while remaining intact [35]. Electroporation of cells on nanostraws increases cargo delivery, for example, improving plasmid transfection efficiency from 5–10% to 60–70% [3, 65]. The electroporation step briefly disrupts the membrane, which can then reseal around nanostraws that have penetrated the cell. Melosh and colleagues used nanostraws to deliver cell-impermeant molecules called azido sugars into cells in order to map protein glycosylation [67]. Loading cells with azido sugars allowed modified glycoproteins to be detected by fluorescent probes conjugated with click chemistry. Other cell-impermeable metabolite or analogue probes, such as modified ATP or synthetic cross-linkers, could be delivered to the cytosol this way [64] (Fig. 5e).

4 Delivery of Probes for Multiplexed Biosensing

In addition to combining cargo delivery and sensing, nanoneedles are now being used for multiplexed cancer marker detection. Biodegradable Si nanoneedles were recently used to deliver multicomponent, enzymatically active probes to detect both miRNA and protein cancer biomarkers using rolling circle amplification and fluorophore-coupled nucleotide probes [68] (Fig. 6). Rolling circle amplification (RCA) is a process in which a short nucleotide primer is amplified to form long single-stranded DNA or RNA molecules through the action of unique polymerases. The whole RCA process can take place at 37°C in a complex biological environment, such as a cell. Mesoporous Si nanoneedles, about 1 μm long and 100 nm in diameter, were fabricated using metal-assisted chemical etching and functionalized with (3-Aminopropyl) triethoxysilane (APTES), a silicon-binding surface chemistry that is frequently used to promote the attachment of probes and biocargos. The nanoneedles were then detached from the substrate and loaded with nucleotide "padlock" probes, FAM- and Cy5-conjugated oligonucleotide probes,

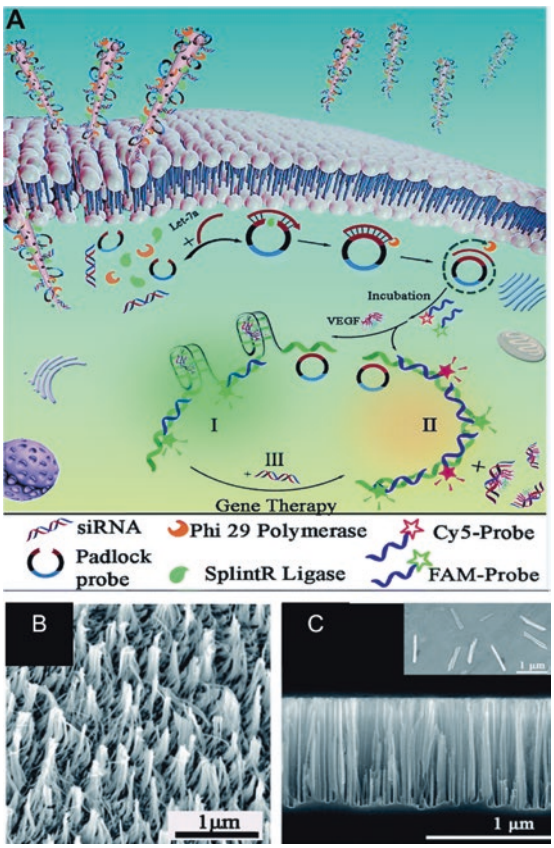

Fig. 6 Porous biodegradable nanosyringes for multiplexed biosensing. (**a**) One-step intracellular rolling circle amplification (RCA). Upon delivery of the "padlock probe," binding of Let-7a miRNA leads to ring formation catalyzed by splintR ligase, followed by amplification catalyzed by phi29 polymerase. An aptamer structure that binds VEGF was designed in the middle of the padlock probe to form a quadruplex in the presence of the protein. In leukemia cells with both Let-7a and VEGF, the RCA products hybridize with the FAM probe, resulting in a green fluorescence (I). In the absence of VEGF, both the Cy5 probe and the FAM probe hybridize to the amplification products, leading to orange fluorescence (II). Cells loaded with siRNA against VEGF therefore showed orange emission due to downregulation of the protein (III). (**b**) SEM top-sectional view of nanoneedles before detachment. (**c**) SEM cross-sectional view of nanoneedles before and after detachment (inset). (Adapted with permission from [68]. Copyright 2019, The Royal Society of Chemistry)

and polymerase and ligase to amplify the padlock probe in the presence of Let-7a miRNA. The padlock probe also contained an VEGF-binding aptamer sequence. The resulting "nanosyringes" were taken up by endocytosis and dissolved within 16 h, similar to porous nanoneedles fabricated by Stevens and colleagues [1, 11, 28, 69]. In the presence of Let-7a transcript and VEGF protein, amplification of the padlock probe and binding to targets produced a green fluorescent signal, whereas in the absence of VEGF, the interaction of FAM and Cy5 produced an orange fluorescent signal. The nanosyringes were also loaded with siRNA targeting VEGF, which resulted in decreased VEGF protein signal due to transcript depletion. Let-7a and VEGF were detected in vitro in cell uptake experiments and in vivo following injection into mouse xenograft tumors. These studies demonstrate the efficacy of using nanoneedles to detect nucleotides and proteins inside cells as part of a multiplexed strategy for tumor detection and gene therapy.

5 Delivery of Nanoparticles as Probes

Nanoneedles have been demonstrated to deliver nanoparticles, such as quantum dots and gold nanoparticles, to the cytosol [1, 70]. Nanoparticles have high surface area-to-volume ratios and the capacity for binding multiple probes. Tang and colleagues showed that Au nanoparticles functionalized with multiple molecular beacons could identify four different intracellular mRNA transcripts [71]. They also developed fluorescent nanoprobes that could distinguish normal and cancer cells based on tumor marker mRNA transcripts (TK1 and GalNAc) and matrix metalloproteinases (MMP-2 and MMP-7) [72]. A number of examples of nanoprobes that target specific MMPs and detect their activity in tumors have been reported [73–75], including one that detects both MMP-2 and urokinase-type plasminogen activator, which is upregulated in many cancers [76]. Gold-coated magnetic nanoparticles modified with redox-labeled DNA probes have also been reported as an ultrasensitive detection method for circulating tumor miRNA in blood [77]. These types of metallic particles could be adapted for intracellular electrochemical sensing by nanoinjection or coupling to nanoneedle probes. Additionally, carbon-based nanomaterials can be utilized to sense a variety of analytes, pH, and even temperature [78].

Biocompatible Au or Au-coated nanoparticles are becoming increasingly popular for label-free sensing using surface-enhanced Raman scattering (SERS). SERS provides highly sensitive and rapid detection of molecules and nanoparticles without the necessity of a fluorescent or reactive probe [79–81]. In 2018, Hanif et al. reported the use of gold-coated nanopipettes (~100 nm tips) functionalized with organic nitrile cyanide to measure Fe^{3+} in live cells [82]. In 2019, De Angelis and colleagues used hollow nanoelectrodes to deliver gold nanorods into cells. Biomolecules colocalized with the gold nanorods could then be detected by the enhanced localized Raman scattering [83] (Fig. 5f). Another novel combination of nanopipettes, nanoparticles, and Raman spectroscopy was reported the same year as a way to measure hypoxia in cells and tumors [84] (Fig. 7). In this study, sharp-edged gold nanostars were coupled to nanopipettes, and SERS was used to measure intracellular redox potential. Clear differences in Raman spectra were observed between triple-negative breast cancer cells and non-tumor MCF10A or nonmetastatic cancer cells in response to hypoxia [84]. The gold nanostar-loaded nanopipettes were then demonstrated to be able to detect hypoxic regions in 3D cell culture and, importantly, in subcutaneous tumors in mice [84]. Nanoneedle-mediated nanoparticle delivery combined with SERS offers a powerful set of tools for cancer research in vitro and tumor detection in vivo.

6 Nanoneedle-Bound Optical Probes

Optical probes can be chemically conjugated to nanoneedles to act as biosensors [85]. An early example of this strategy used a cleavable FRET probe conjugated to an AFM nanoneedle (400 nm tip) to detect caspase-3 activation in live cells [86]. Here, a change in the FRET signal was observed when the Alexa546 fluorophore was cleaved from the GFP portion of the probe by active caspases in apoptotic HeLa cells. Caspase-cleavable fluorescent probes were also used in a nanoneedle "sandwich assay," in which cells held in place on an adherent nanoneedle array were interfaced with Si nanoneedle arrays decorated with covalently linked TAMRA-labelled peptides [87] (Fig. 8a). In the presence of active caspase in the cytosol, the TAMRA tag was cleaved, resulting in red fluorescence in the cells after removal of the probes (Fig. 8b). In the same study, the sandwich assay was used to monitor protein tyrosine phosphatase (PTP) and protein kinase A (PKA) activity in cells by inserting nanoneedles conjugated with peptide kinase/phosphatase substrates. In the latter cases, however, peptide phosphorylation was determined by MALDI-TOF mass spectroscopy rather than fluorescence [87]. Nakamura and colleagues used fluorescent molecular beacons coupled to arrays of Si nanoneedles by biotinylation to detect GAPDH mRNA [88, 89]. Similar to the sandwich assay [87], nanoneedles were inserted into the apical side of adherent cells. However, in the latter study, penetration was controlled by piezoelectric-driven oscillating mechanism so that force and depth could be precisely controlled, and interfacing times with cells were much shorter (10–30 minutes compared with 24 h) [89].

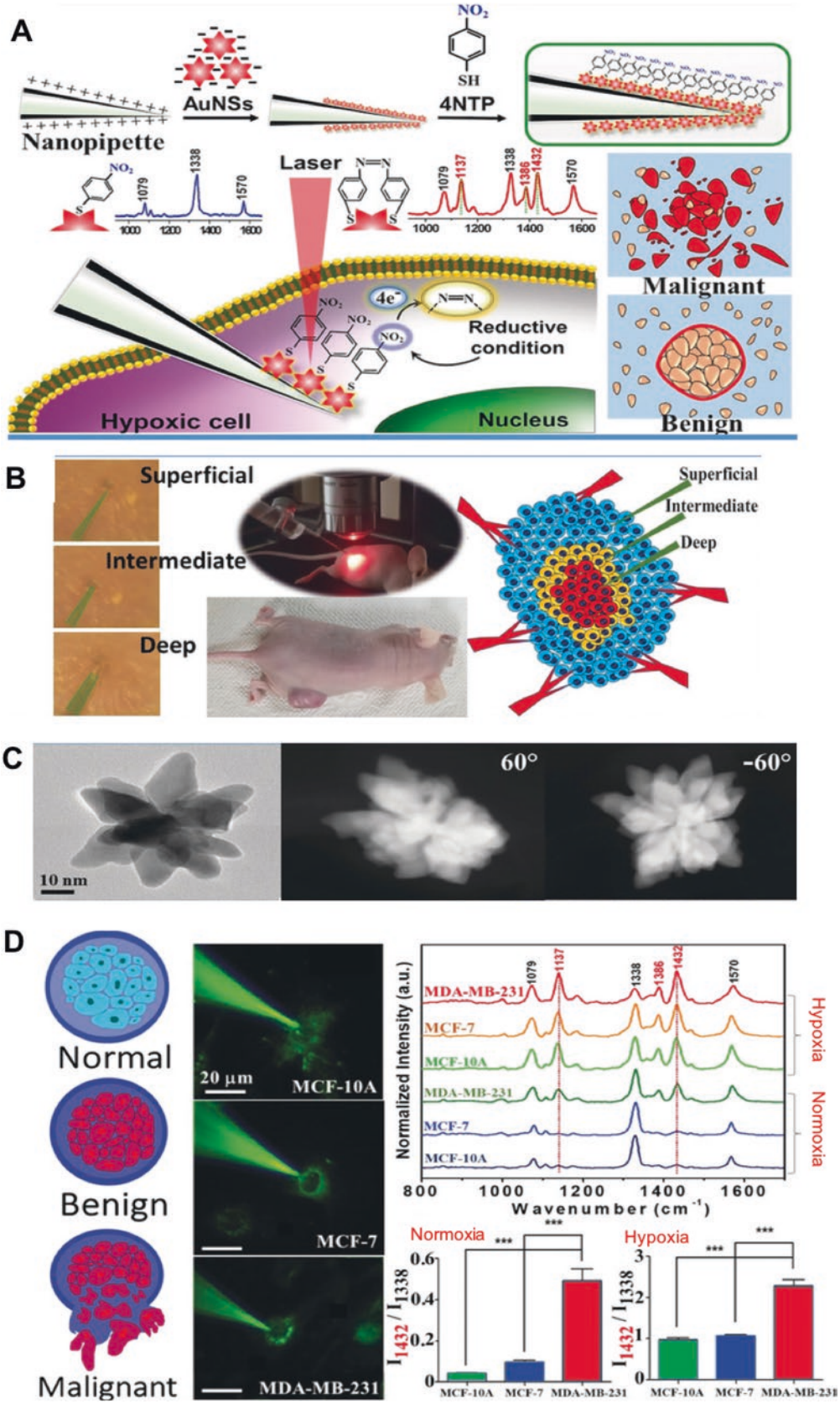

Fig. 7 Raman-based hypoxia detection using a nanopipette and gold nanostars. (**a**) Schematic of the working principle. Gold nanostars were assembled on nanopipette tips and functionalized with 4-nitrothiophenol (4NTP). Spectral changes for the 4NTP redox group (nitro-NO_2) resulting from intracellular oxygen were quantified. (**b**) In vivo detection of hypoxia in different regions of subcutaneous mouse tumors using the gold nanostar probe. (**c**) 2D TEM and 3D tomography images of Au nanostars showing spikes at tilt angles −60° and 60°. (**d**) Raman probes were used to measure spectra in normal breast myoepithelial cells (MCF10A), nonmetastatic breast cancer cells (MCF7), and metastatic breast cancer cells (MDA-MB-231) under normoxia and hypoxia. (a) Raman probe interacting with cells. (b) Surface-enhanced Raman spectra for cells in each condition. (c) Quantification of peak ratios that are indicative of changes in redox state inside cells (***$p < 0.001$). (Adapted with permission from [84]. Copyright 2019, Wiley)

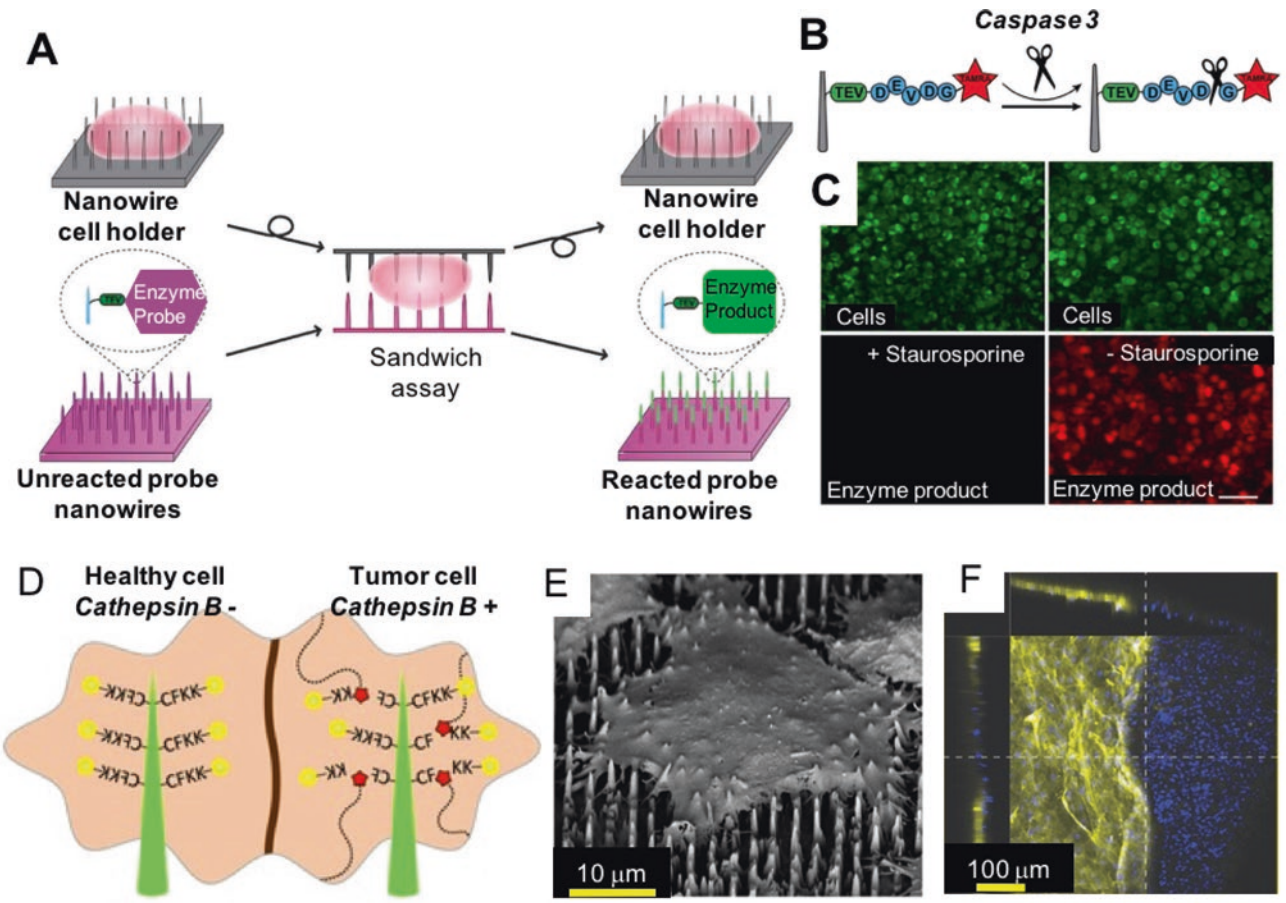

Fig. 8 Nanoneedle-bound optical probes. (**a**) Nanoneedle "sandwich assay." Cells are immobilized on the one nanoneedle array. Then another array, functionalized with a bound caspase-3 probe (**b**), is interfaced with the cells. When the fluorescent-labeled peptide that immobilizes on the nanoneedles is in contact with active caspase-3 in cells, the red probe is released into the cytoplasm. (**c**) Cells are labeled in green (top). Caspase-3 activity is indicated by red fluorescence in cells treated with staurosporine, which induces apoptosis (bottom). (Adapted with permission from [87]. Copyright 2013, American Chemical Society). (**d**) Porous Si nanoneedle (green) arrays functionalized with the cathepsin B (CTSB) probe (yellow) interface with cells, either by seeding directly on top of the nanoneedle arrays or by pressing against tissue samples. When CTSB (red) is active, the fluorescent probe is cleaved from the peptide substrate. (**e**) A cell growing on a nanoneedle array (SEM). (**f**) Esophageal tissue stamped with nanoneedle biosensor on the tumor margin. Yellow fluorescence indicates CTSB activity in the tumor region. (Adapted under the terms of CC BY license from [10]. Copyright 2015, The Authors)

7 Nanoneedle-Bound Probes for Cancer Biomarkers

Nanoneedles with covalently bound molecular probes have been reported for measuring intracellular pH and enzymatic activities in cancer cells. Dysregulation of pH homeostasis is a common characteristic of tumor cells, which often have higher intracellular pH and lower extracellular pH than healthy cells [90]. Intracellular pH has been measured using nanoneedles with optical and electrochemical functionalization. Chiappini and Stevens used porous Si nanoneedles (tips <100 nm) conjugated with a pH-sensitive fluorophore and a reference fluorophore to measure the pH of interfaced cells by ratiometric imaging. Cells can be injected either from the bottom-up by seeding directly on top of the nanoneedles, or from the top-down by pressing the nanoneedle array against the apical surface [1], which was previously shown not to impair cell viability [11]. Chiappini et al. also used a cleavable TAMRA-peptide probe to sense cytosolic cathepsin B (CTSB) in order to detect cancer cells seeded on Si nanoneedle arrays [10] (Fig. 8d–e). CTSB is a cysteine protease that is a cancer biomarker associated with poor prognosis in many solid tumors [91]. Transformed cells could be distinguished from normal cells in a mixed population based on cleavage of TAMRA by fluorescence microscopy. Furthermore, when nanoneedle sensors were applied to human tissue samples, high CTSB activity was revealed by fluorescence in esophageal tumors and in regions diagnosed by histopathology as having premalignant Barrett's dysplasia (Fig. 8f). Application of the nanosensor array to a tumor margin also showed clear demarcation between diseased and healthy tissue [10]. Proteolytic CTSB activity has

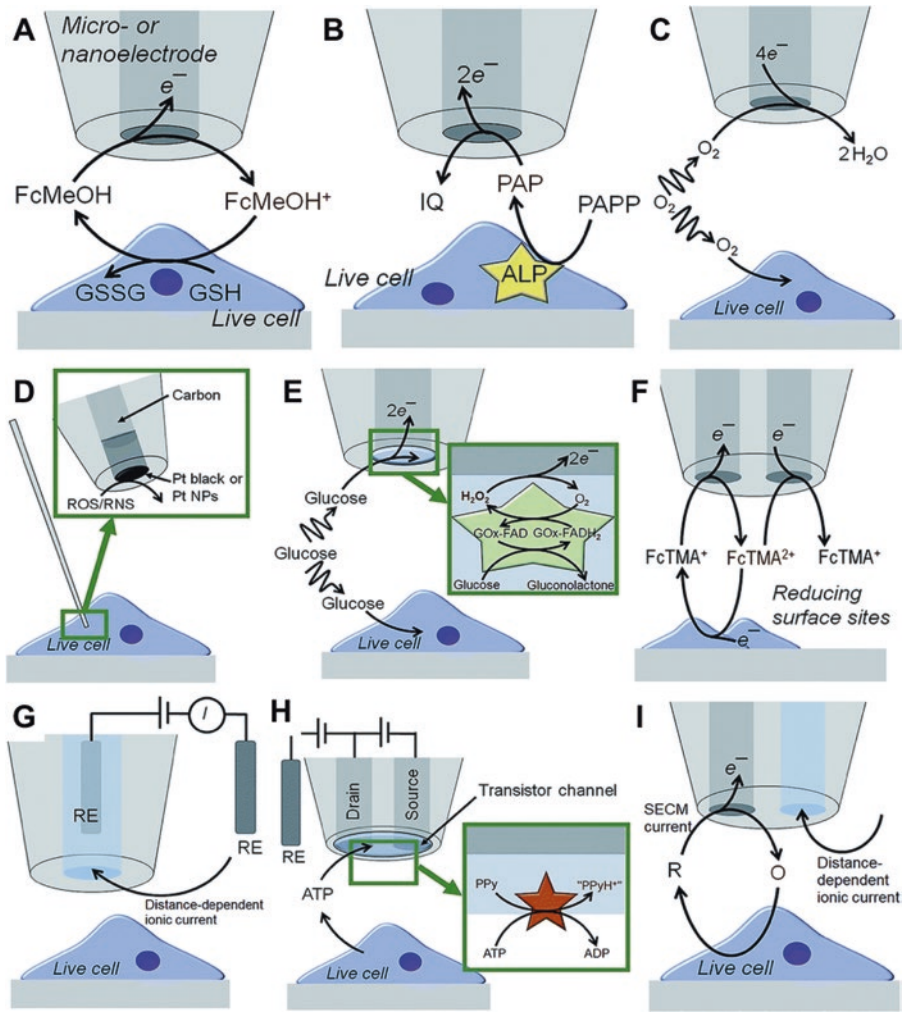

Fig. 9 Schematics of the operating principles of typical electrochemical scanning probe microscopy electrodes. (**a**) SECM feedback (FB) mode. (**b**) SECM substrate generation/tip collection (SG/TC) mode. (**c**) SECM redox (RC) competition mode. (**d**) Pt-based nanoelectrode for noninvasive intracellular recordings. (**e**) Microbiosensor for specific metabolite detection. (**f**) Dual electrode SECM tip. (**g**) SICM for topographic mapping. (**h**) Nano-FET for specific metabolite detection. (**i**) SECM-SICM for constant distance mode electrochemical imaging. (Reproduced under the terms of CC BY license from [94]. Copyright 2018, The Royal Society of Chemistry)

also been measured using peptide-coupled nanoelectrode arrays in breast cancer cell lysates [92].

8 Nanopipette Electrodes to Monitor Cell Metabolism

Nanocapillary electrodes have been used to monitor changes in cell metabolism, which are hallmarks of cancer biology [93]. The range of nanoelectrode varieties used to measure analytes via redox chemistry is summarized in Fig. 9 and reviewed in depth by Lin et al. [94]. For recent reviews of nanoelectrode fabrication, see [58, 95].

Nanocapillaries can be used to deliver unbound probes that produce electrochemically active analytes, such as hydrogen peroxide. Chen and colleagues report delivery of "nanokits" comprised of commercial enzymatic assay components into cells, where metabolites are detected via H_2O_2 generation [96, 97]. They used glass nanocapillaries fabricated with Pt ring electrodes with tips ~200–300 nm in diameter and tip openings of ~130 nm [96]. These nanocapillaries were used to deliver femtoliter quantities of 1) glucose oxidase to detect glucose in HeLa cells and 2) a cocktail of sphingomyelin, alkaline phosphatase, and choline oxidase to measure sphingomyelinase activity in J774 macrophage-like mouse reticulum sarcoma cells [96, 97]. After nanocapillary insertion, voltage was applied to induce electroosmotic flow, resulting in the capillary contents being pumped into the cytosol. Enzymatic reactions that occurred in the vicinity of the electrode were limited by diffusion, so analyte detection was spatially localized [97]. At the same time, intracellular calcium concentrations were measured fluorometrically using Fluo-3. Ca^{2+} did not change significantly during nanocapillary insertion or voltage application, indicating that cells were functioning normally. In another study, Pan et al. used nanocapillary ring electrodes to deliver the contents of an ion assay kit comprised of maltose phosphorylase, maltose, mutarotase, and glucose oxidase into HeLa cells to mea-

sure intracellular phosphate ion concentrations [98]. Electroosmotic flow through quartz nanocapillaries with ~100 nm tips has also been employed for ultrafast monitoring of mitochondrial membrane potential in MCF7 breast cancer cells [99]. In this study, Qian and colleagues applied a voltage to inject cells with inactive fluorescent dyes or JC-10, which selectively accumulates in mitochondria and reversibly changes from green to red as membrane potential increases. Red fluorescence, indicating mitochondrial activity, was observed within 20 s after nanoinjection, compared with 20–30 minutes for passive loading by incubation in aqueous JC-10 solution. This method detected rapid changes in mitochondrial metabolism in single cells in response to metformin, a drug used in diabetes and cancer treatment that inhibits mitochondrial electron transport complex I [100].

Over the past 10 years, Pourmand and colleagues have developed a variety of nanopipette electrode probes functionalized with biomolecular sensors to measure a number of metabolic processes implicated in cancer in single cells [6]. In 2015, they reported a method for monitoring intracellular pH using single-cell nanoprobes (tips <100 nm) [101]. These nanoprobes were comprised of quartz nanopipettes coated with chitosan, a polysaccharide biopolymer that undergoes reversible structural changes depending on pH [102], and coupled to a potentiostat with Pt wire. Changes in the ionic current at the nanopipette tip are detected by the electrode as rectification of the output current measured by the system, when stimulated by an oscillating input voltage signal [103, 104]. Nanoprobes were inserted into cells using a custom-built scanning ion conductance microscope. Changes in pH could be monitored in real time as cells were treated with a Cl^- channel blocker, and cytosolic pH measurements were found to be lower in cancer cells than in healthy fibroblasts. The Pourmand group also developed nanopipettes modified with glucose oxidase (GOx) as single-cell, real-time glucose sensors [105] (Fig. 10a–e). In the presence of glucose, GOx activity leads to the production of hydrogen peroxide and current rectification is detected by the nanoelectrode. These studies revealed cell-to-cell variations as well as differences between cell lines, with cancer cells having higher levels of intracellular glucose and increased rates of glucose uptake than normal fibroblasts.

A common feature of cancer cells is switching from oxidative phosphorylation to anaerobic respiration as their main means of ATP generation, which is called the Warburg effect [106]. The final step of glycolysis is the conversion of pyruvate to lactate. A carbon fiber microelectrode coated with lactose oxidase mixed with chitosan, deposited by electrodeposition, was reported to detect lactate fluctuations in brain tissues via H_2O_2 production [107]. This type of probe could also be adapted for intracellular glycolysis measurements. Korchev and colleagues have developed nanometer-scale dual carbon electrodes (DCE) for high-resolution sensing and topological mapping [108]. The addition of polypyrrole (Ppy) to the DCE nanopipette tip enhanced pH sensing and temporal resolution, and the spear shape enhanced spatial resolution. This group also reported a similar spearhead probe consisting of hexokinase immobilized on a pH-sensitive Ppy nano field-effect transistor (FET) as selective ATP biosensor [109] (Fig. 10f). Hexokinase cleavage of ATP leads to a stoichiometric generation of protons, which is detected as a localized change in pH. Thus, carbon nanoelectrodes have many potential applications for investigating oxidative metabolism of living cells.

A new class of nanocapillary probes termed asymmetric nanopore electrodes (ANE) were reported to enable real-time sensing of cellular respiration in breast cancer cells and were used to monitor the effects of anticancer drugs on cell metabolism [110] (Fig. 11). Instead of a wire sealed in the electrode, the ANE's interior is coated with Au and acts as the redox sensing interface which has high temporal and spatial resolution. The tip (~90 nm) of the gold interior of the nanocapillary is polarized as the cathode, and the opposite terminal acts as the anode; an ionic current is generated when the reducing agent NADH diffuses into the tip. Importantly, the ANE was modified with electrochemically reactive 4-thio-catechol (4TC). Reduction of 4TC at the tip led to the generation of H_2 nanobubbles and thus amplified the signal severalfold. Intracellular NADH was measured inside live MCF7 breast cancer cells, and decreases in NADH induced by taxol treatment were reliably detected. This method could be extended to other redox sensors using either reduction-induced H_2 or oxidation-induced O_2 nanobubbles.

9 Multimodal Fluorescent and Electrochemical Detection of mRNA

A multimodal strategy for mRNA detection was reported by Huang et al., who developed "signal-on" or "signal-off" assays based on photocleavable molecular beacons to detect manganese superoxide dismutase (MnSOD) transcripts in MCF7 breast cancer cells in [111] (Fig. 12). MnSOD, or SOD2, is a mitochondrial enzyme that regulates the metabolism of reactive oxygen species (ROS), converting superoxide into hydrogen peroxide. High MnSOD expression is a common feature of tumor cells and is associated with the switch to glycolysis [112]. These experiments used nano fiber-optics to selectively irradiate cells and nanopipettes to record electrochemical signals. In the "signal-on" experiments, single cells were irradiated with UV light, which led to spatially localized activation of DNA probes. The probes consisted of two oligonucleotides, one with a green fluorophore and the other with a red fluorescent quencher. The quencher also contained a photocleavable hairpin. Upon irradiation, the quencher could be displaced from the signal probe, leading to an increase in green fluorescent signal (Fig. 12a, b). In the "signal-off" assays, a nanoelectrode was conjugated to a thiol-modified oligonucleotide and comple-

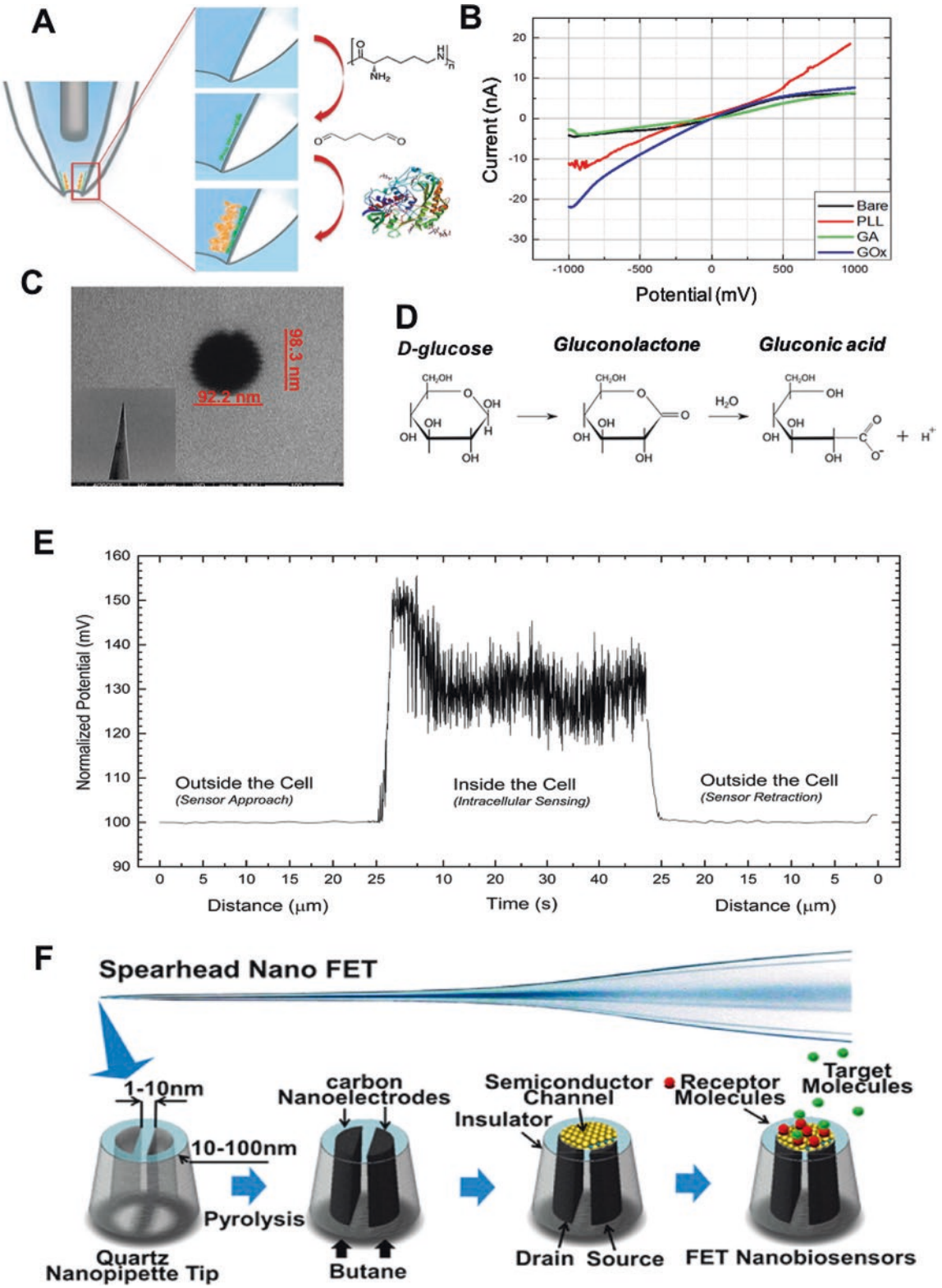

Fig. 10 Single-cell metabolic nanosensors. (**a**) Schematic of surface modifications for the immobilization of glucose oxidase in the nanopipette tip. The inner surface is coated with poly-L-lysine (PLL) and then treated with glutaraldehyde to cross-link the amino group of PLL to glucose oxidase (GOx). (**b**) Electrochemical characterization of the nanopipette after each step in the fabrication process. (**c**) SEM image of the nanopipette tip. Inset: side view of the nanopipette. (**d**) The chemistry of enzymatic conversion of glucose to gluconic acid. (**e**) Single-cell readings using the glucose nanosensor. As the sensor tip approaches the cell membrane, the potential increases sharply. Once the tip has penetrated the cytoplasm, the potential drops to a steady state of fluctuations caused by localized peroxide generation. After the nanopipette is withdrawn, the potential drops back to baseline. (Adapted with permission from [105]. Copyright 2016, American Chemical Society). (**f**) Spearhead nano-FET. A nanometer-scale field-effect transistor was fabricated by deposition of a thin layer of semiconductor material (polypyrrole) on the tip of dual carbon electrodes, made by pyrolytic decomposition of butane, that serve as drain and source. Redox-generating molecules (e.g., hexokinase) immobilized on the transistor provide selective FET sensing. (Reproduced with permission from [109]. Copyright 2016, American Chemical Society)

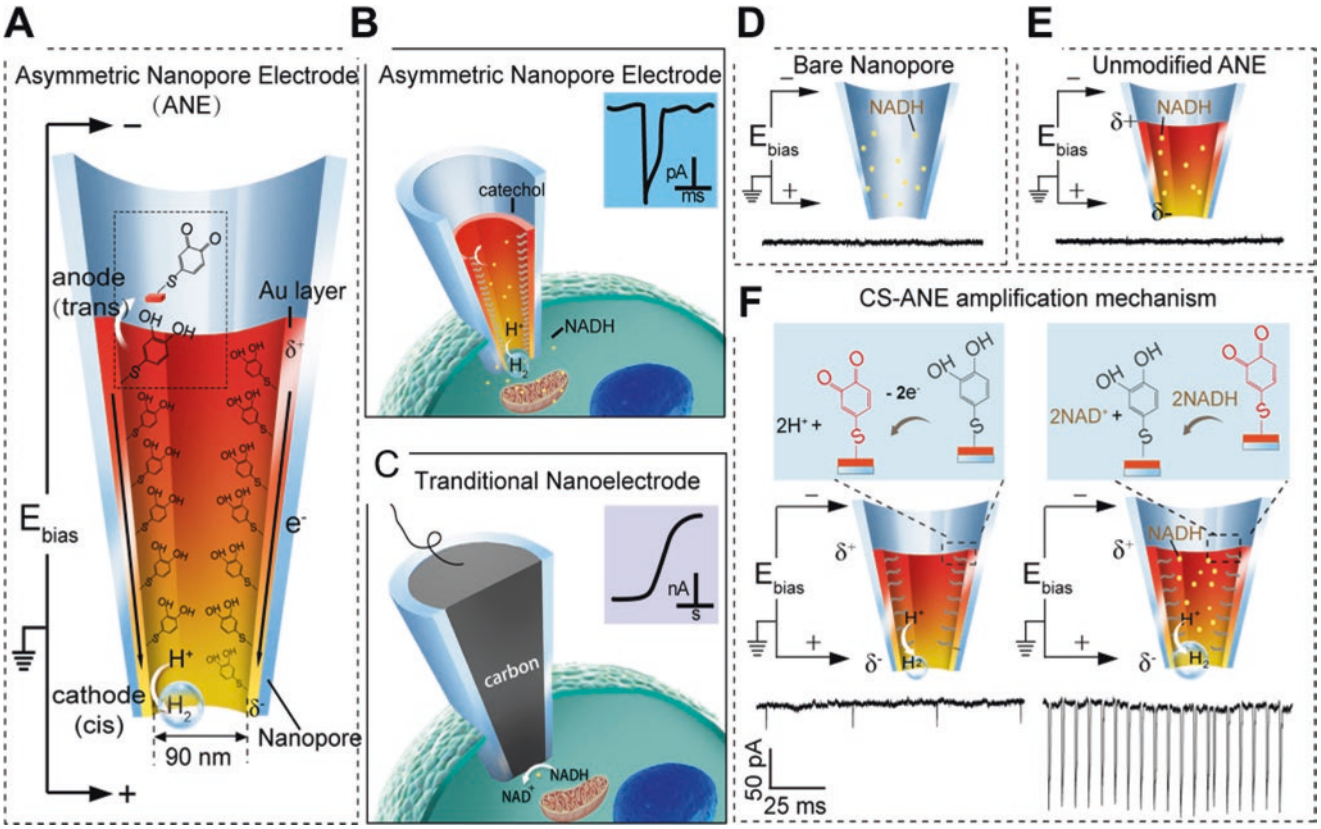

Fig. 11 Wireless asymmetric nanopore electrode (ANE) for real-time sensing of cellular respiration. (**a**) Schematic of the ANE. The applied bias potential drives the potential difference between the two terminals of the Au- and 4-thiol-catechol (4TN)-coated nanopores. The tip opening (*cis*) is polarized as the cathode and the opposite terminal (*trans*) acts as the anode. Reduction occurs at the cathode and oxidation occurs at the anode. (**b**) Intracellular redox species (e.g., NADH) diffuse into the *cis* tip of the ANE, and a pair of redox reactions takes place at the cathode and anode. A transient ionic current response is generated (inset) which allows a high degree of temporal resolution. (**c**) Traditional carbon nanoelectrode schematic with a solid tip that generates a cyclic voltammogram (inset) with poor temporal resolution. (**d**) The bare nanopore does not produce any current in response to NADH. (**e**) The unmodified ANE generates a stable baseline signal. (**f**) The 4TN-coated ANE generates an enhanced current signal due to the generation of H_2 bubbles at the cathode. Left: 4TN is oxidized electrochemically at the anodic pole while a small amount of H_2 is produced at the cathodic pole, generating a weak signal. Right: in the presence of NADH, the catechol conversion is mediated by the redox pair NADH/NAD+, leading to the production of H_2 bubbles and an amplified current response. (Reproduced with permission from [110]. Copyright 2018, American Chemical Society)

mentary methylene blue (MB)-modified hairpin probe. In the absence of irradiation and target mRNA, the nanoelectrode signal was high due to MB redox. When the hairpin was cleaved and MnSOD mRNA was present, displacement of the MB led to depletion of the electrical signal (Fig. 12c, d) [111].

10 Nanopipette Electrodes to Monitor Reactive Oxygen Species Generation

Metabolic reprogramming in cancer leads to changes in the production of ROS and oxidative stress [113, 114]. Platinized carbon nanoelectrodes have long been used to investigate cellular redox chemistry and ROS generation. Pt black is a fine powdered form of Pt that is widely used for improving electrode efficiency by greatly increasing the reactive surface area. Early studies of single-cell ROS detection were performed by Amatore and colleagues in the 1990s using platinized carbon fiber microelectrodes, but cells had to be punctured to release their contents [115]. In 2008, Mirkin and colleagues reported the use of platinized glass nanoelectrodes with ~40 nm tips in diameter to perform intracellular voltammetry in living MCF10A non-tumor breast epithelial cells [116]. Scanning electrochemical microscopy (SECM) [24] was used to position the tip of the electrode, map cell topography, measure membrane potential, and detect redox reactivity inside cells. A current was observed when the probe was in the hydrophilic redox buffer outside the cell and disappeared when the tip penetrated the plasma membrane, indicating that the membrane had resealed around the probe and was not leaky. A redox buffer containing $Ru(NH_3)_6^{3+}$, which cannot cross the plasma membrane, is commonly used to confirm cell penetration and membrane resealing in nanoelectrode studies. SICM-coupled carbon nanoelectrodes functionalized with Pt were reported in 2014 by Korchev and colleagues, who fabricated disk-shaped

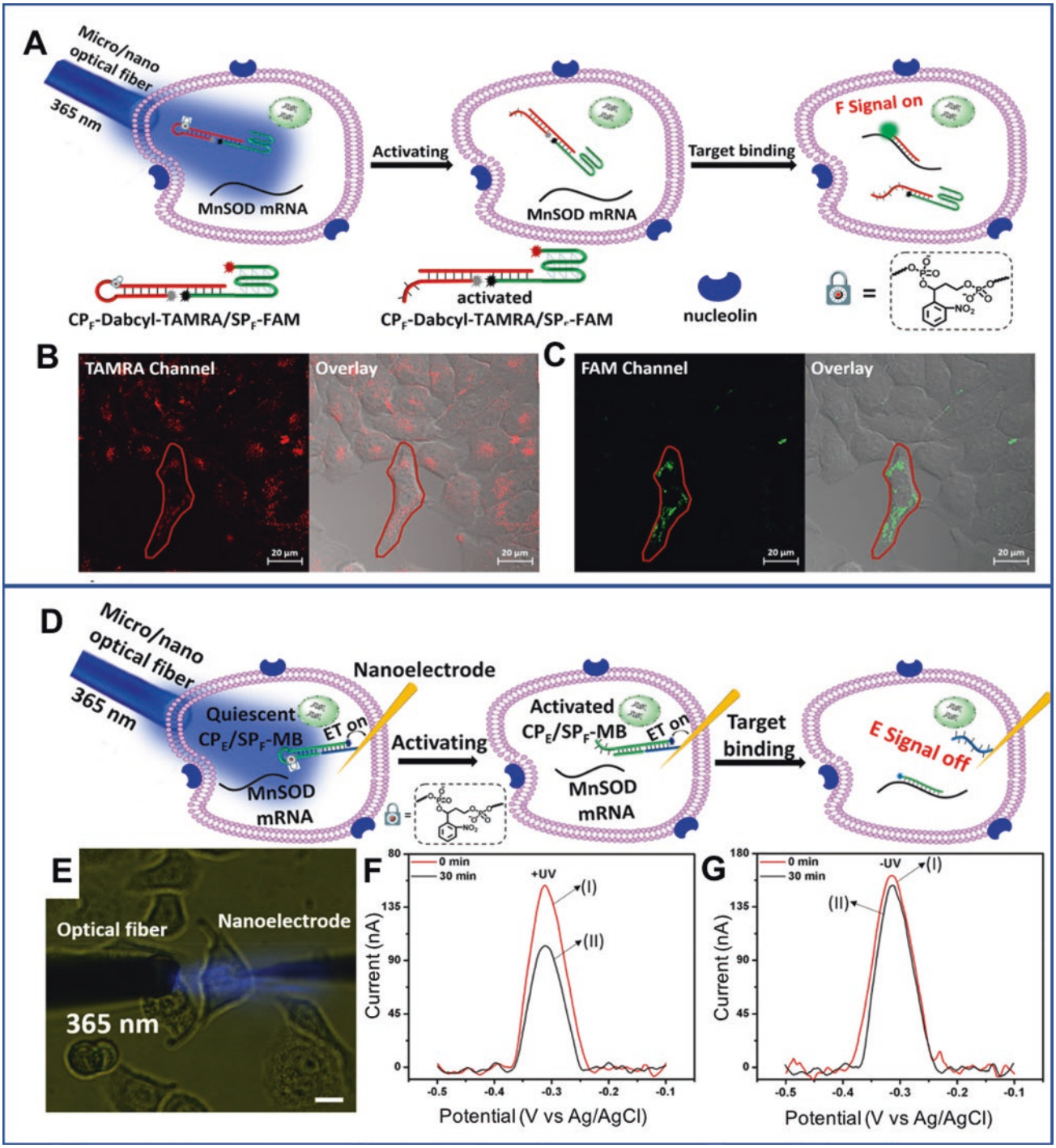

Fig. 12 Multimodal mRNA detection of MnSOD mRNA in MCF-7 breast cancer cells. Top box: the "signal-on" strategy. (**a**) Principle of the photoactivated toehold-mediated displacement reaction for the optical mRNA sensing probe. The probe consists of an oligonucleotide with a green fluorophore (FAM), conjugated to a cell surface receptor-binding aptamer, and a hairpin oligonucleotide carrying a quencher red fluorophore (Dabcyl-TAMRA). The hairpin is photocleavable due to the inclusion of an o-nitrobenzylphosphate linker. Binding of the probe aptamer to nucleolin facilitates uptake by cancer cells. A single cell is irradiated with UV light using a micro or nano optical fiber to cleave the probe hairpin, allowing the FAM probe to bind to complementary mRNA. This association displaces the quencher, resulting in green emission from the fluorophore. (**b**) Red TAMRA fluorescence shows uptake of the probe in all cells. (**c**) Green fluorescence is observed only in the photoactivated cell (red line). Bottom box: the "signal-off" strategy. (**d**) Schematic of the electrochemical mRNA sensing probe. The nanoelectrode is functionalized with a thiol-modified capture probe (CP_E) which is bound to a complementary methylene blue (MB)-modified photocleavable hairpin signal probe (SP_E-MB). When the hairpin is cleaved upon UV irradiation in the presence of target mRNA, the electrochemical signal at the nanopipette decreases. (**e**) Micrograph of cells under illumination with intracellular nanoelectrode probe. (**f**) Voltammetric response of a single cell before (I) and after (II) 30 min of UV irradiation. (**g**) Voltammetric recordings of a single cell at 30-min intervals without irradiation. (Adapted with permission from [111]. Copyright 2018, American Chemical Society)

carbon electrodes with radii as small as 5 nm [108]. These nanoelectrodes were used to measure O_2 consumption in brain tissue explants and inside single melanoma cells. In 2018, Pourmand and colleagues used SICM-coupled nanopipettes (~40 nm pore) to specifically detect superoxide (O_2^{*-}) in living cells [117]. These nanoprobes were covalently modified with cytochrome-c, an electron acceptor that converts O_2^{*-} to O_2. Current rectification was sensed by the coupled electrode in the presence of O_2^{*-}. Superoxide levels increased as expected in MCF10A breast myoepithelial cells exposed to carbonyl cyanide 3-chlorophenylhydrazone, a protonophore that induces the generation of ROS in mitochondria, and adding superoxide dismutase (SOD), a ROS scavenging enzyme, had the opposite effect.

Much of the recent work on detecting ROS in live cells has been performed using macrophages, which produce superoxide both to combat pathogens and as part of the monocyte differentiation process [118]. In the former scenario, a macrophage subjects an engulfed pathogen to an intense burst of ROS and reactive nitrogen species (RNS) contained in vacuoles called phagolysosomes, and the debris and leftover ROS/RNS are then ejected from the cell. In the latter, tumor-associated macrophages take on a chronic inflammatory phenotype due in part to the superoxide-mediated signaling. Amatore and colleagues used Pt black-coated nanoelectrodes (>100 nm tips), fabricated using a novel AFM-controlled method, to detect ROS/RNS in live macrophages [119]. However, these probes lacked specificity as the applied potential could oxidize other compounds, such as uric acid. Carbon electrodes coated with the electrocatalyst Prussian Blue were reported to more selectively detect hydrogen peroxide in mouse macrophages [120]. Rawson et al. used single-walled carbon nanotubes (SWCNTs) functionalized with an osmium catalyst, osmium bipyridine (Osbpy), to specifically detect H_2O_2 production in RAW 264.7 cells stimulated with lysophosphatidic acid (LPS) [121] (Fig. 13). Here, the SWCNT electrodes were interfaced with cells by centrifugation. LPS stimulation led to generation of intracellular ROS, and electron transfer from Osbpy to ROS resulted in a drop in current at the nanoelectrode (Fig. 13a). This process could be blocked by the addition of ROS inhibitors (Fig. 13b, c). In 2020, a novel tungsten nanoelectrode was used to selectively measure hydroxyl radicals (*OH) in RAW 264.7 macrophages [122]. Tungsten wires were etched to conical nanoneedles and sheathed with Au nanoparticles and then coated with a self-assembled monolayer of 1-hexanethiol, which blocked the electrochemical signal until attacked by *OH. Hoechst 33258 and MitoTracker were used to label cellular organelles and establish the subcellular positioning of nanoelectrodes. Hydroxyl bursts were observed following stimulation with LPS. Interestingly, the *OH bursts were many times lower inside cell nuclei than in the cytosol and twofold higher in close proximity to mitochondria, which suggests that these ROS were by-products of mitochondrial respiration.

Two recent studies used nanoelectrodes to measure ROS/RNS specifically inside phagolysosomes of living macrophages [123, 124]. Zhang et al. used cylindrical silicon carbide nanowire electrodes (300–500 nm diameter) inserted into RAW 264.7 macrophages to detect intracellular ROS/RNS. They recorded transient spikes in current, which were determined to be phagolysosomes colliding with the nanowire. A similar study was performed using carbon fiber nanoelectrodes to measure neurotransmitter contents in PC12 cells [125]. Hu et al. also probed RAW 264.7 macrophages but used smaller platinized carbon nanopipettes (tip <100 nm) and distinguished four species of analytes (H_2O_2, $ONOO^-$, NO^*, and NO_2^-). This was accomplished by recording currents over a periodic sequence of potentials, because each ROS/RNS is oxidized at a different potential. Besides investigating macrophages, Mirkin and colleagues previously used similar platinized carbon nanoelectrodes to measure the contributions of four ROS/RNS in non-tumour (MCF10A) and triple-negative breast cancer cell lines (MDA-MB-231 and MDA-MB-468) [126]. They found that ROS/RNS levels were lowest in the non-tumor and highest in the MDA-MB-231 cells. They then measured ROS generation in MCF10A cells treated with diacylglycerol (DAG)-lactone, which induces the activation of protein kinase C (PKC), which is overexpressed in many human breast tumors. A series of oxidative bursts were recorded from about 25 minutes after DAG-lactone addition, suggesting that PKC activity induces oxidative stress which in turn drives cancer malignancy.

11 Nanoelectrodes for Metal Ion Detection

Metal-sensing-functionalized nanoelectrodes show promise as intracellular probes for cancer research. For example, many important signaling pathways that are involved in tumor growth and metastasis rely on calcium ions, such as cell adhesion and actomyosin dynamics [127]. The Pourmand group used nanoprobes conjugated with immobilized calmodulin, a Ca^{2+}-binding protein, to measure extracellular calcium ions [4]. Intracellular calcium ion detection was also achieved by Son et al. using SWCNT FETs in nanocapillaries [128]. The SWCNTs were functionalized with Fluo-4-AM dye, which acted as both an electrochemical sensor for Ca^{2+} binding and as a fluorescent probe.

Although they have not yet been used in living cells, biomolecule-coated quartz nanocapillary electrodes have been developed to measure the levels of various other metal ions in solution. Iron plays a key role in aerobic respiration and ROS generation, and dysfunctional iron metabolism has

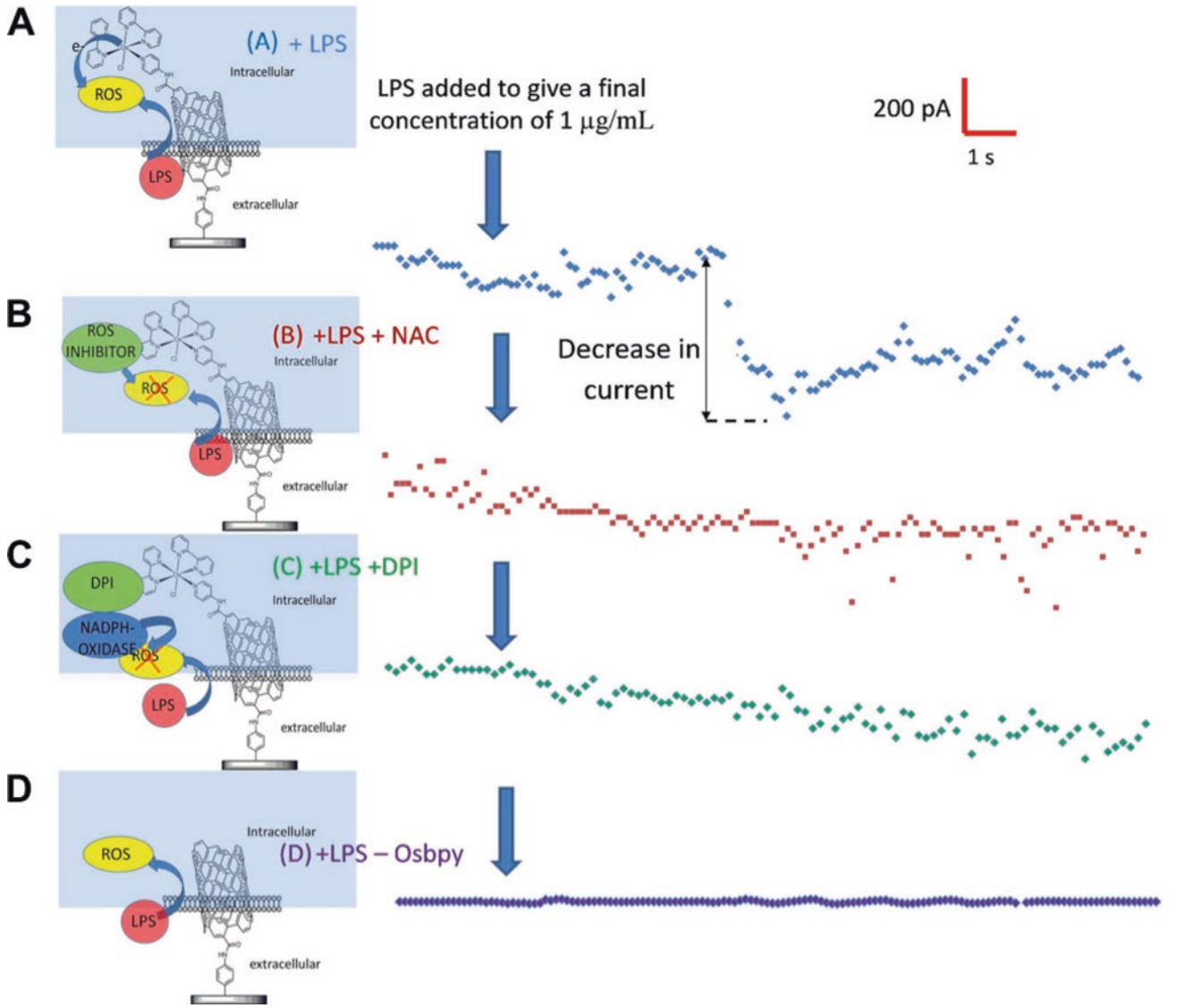

Fig. 13 Reactive oxygen species measurements in live macrophages using single-walled carbon nanotube (SWCNT) probes. Typical current amperograms over time measured in RAW 264.7 macrophages interfaced with SWCNT functionalized with osmium bipyridine (Osbpy) (**a**–**c**) or without functionalization (**d**). (**a**) Addition of LPS induces the generation of ROS. Electron transfer from Osbpy to ROS results in a rapid decrease in current. (**b**, **c**) ROS generation and current decrease is blocked in the presence of ROS inhibitors, N-acetyl cysteine (NAC), and diphenyleneiodonium (DPI). (**d**) No current is observed in the absence of Osbpy. (Reproduced with permission from [121], https://pubs.acs.org/doi/10.1021/acsami.5b06493. Copyright 2015, American Chemical Society. *Further permissions related to the material excerpted should be directed to the ACS*)

been implicated in cancer [129]. An iron-binding protein from *H. influenzae* was used to detect ferrous ions in solution [130]. Other heavy metals also play roles in normal cellular processes and contribute to the production of ROS, DNA damage, inflammation, and tumorigenesis in high concentrations [131, 132]. Divalent copper ion nanopipette sensors have been fabricated from a combination of chitosan and polyacrylic acid [133] and from the copper-binding domain of prion protein [134]. Baker and colleagues used imidazole-modified nanopipettes to measure cobalt ions in solution [135]. An intracellular optical probe could be also adapted from fluorophore-conjugated Si nanowires, which were used to measure free copper ions in liver and HeLa cell lysates by fluorescence quenching [136].

12 Nanoelectrode Arrays for Cell Sensing on the Population Scale

To scale up from the single-cell level, nanoelectrodes can be fabricated as multielectrode arrays (MEA). The majority of these studies have been performed on neuronal cells [137–140] or cardiomyocytes [141], which are the most obvious cell types for electrical assays. It should be noted that the

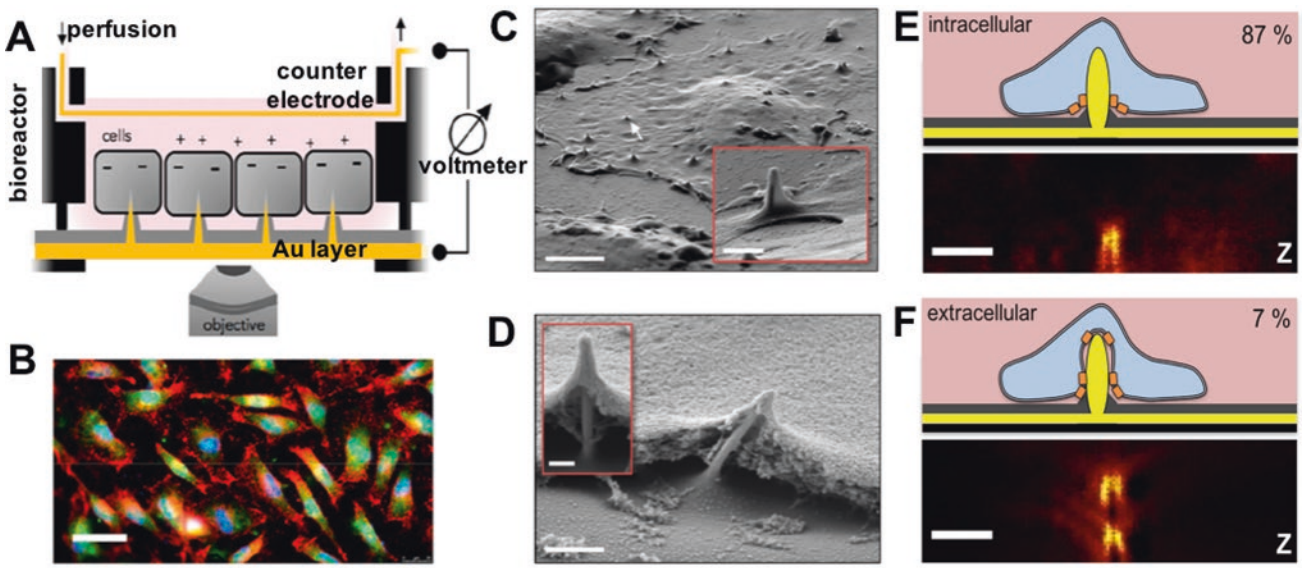

Fig. 14 Gold multielectrode arrays (MEA) used for measuring electrical activity in adherent cells. (**a**) Schematic of the MEA system. (**b**) Fibroblasts seeded on gold nanowire arrays stained to label the plasma membrane (wheat germ agglutinin, red), cytosol (CellTracker, green), and DNA (DAPI, blue). Scale bar = 20 μm. (**c**) SEM images of a fibroblast growing on gold nanowires. White arrow = interfacing electrode. Scale bars = 5 μm and 1 μm (inset). (**d**) SEM images of fracture cross sections of cell-electrode interface. Scale bars = 5 μm and 200 nm (inset). (**e**, **f**) Schematic illustrations (top) and z-projections (bottom) of paxillin staining around nanoelectrodes. In 87% of cases, focal adhesions were only observed around the base of electrodes, and in 7% of cases paxillin was observed along the length of the electrodes. Scale bars = 2 μm. (Adapted with permission from [142], https://pubs.acs.org/doi/10.1021/acs.nanolett.9b00784. Copyright 2019, American Chemical Society. *Further permissions related to the material excerpted should be directed to the ACS*)

majority of systems require cells to be electroporated in situ in order to facilitate intracellular access and sensing of intracellular (rather than extracellular) voltages, which may impart unknown changes on cell electrophysiology. However more recently, en masse electrical activity in electrically coupled cell populations was observed, without the need for electroporation, using Au nanowire arrays in fibroblasts as well as myotubes and neuronal networks [142] (Fig. 14a–d). Cells were found to adhere to the nanowires and remained viable for many days in culture. Paxillin-containing focal adhesions formed around the base or along the side of the nanowires (Fig. 14e, f). The majority of nanowire interfaces had paxillin complexes only at the base, suggesting cytosolic penetration (Fig. 14e). Electrical oscillations recorded by these MEAs were attributed to cellular contractility events involving localized Ca^{2+} waves.

Metal nanoelectrodes can also be combined with SERS to allow both electrical and chemical properties to be sensed from the same cell populations. SERS offers a powerful tool for studying cells interfaced with nanoelectrodes, because Raman spectroscopy provides information about lipids, proteins, and nucleotides. Caprettini et al. plated U2OS osteosarcoma cells on gold MEAs and monitored Raman spectra after electroporation [143]. They detected changes in lipid and amino acid peaks consistent with membrane rupture and resealing and also observed DNA peaks which suggested nuclear penetration or at least nuclear envelope disruption. Mapping physiological and molecular probe-induced electrochemical readouts and Raman spectra from cultured cancer cells or living tissues using MEAs could provide valuable information about cellular activities in wider population contexts.

13 Probing Cytoskeletal Mechanics with Antibody-Conjugated AFM Tips

Cancer cells undergo significant changes in cytoskeletal organization and mechanics. Changes in actomyosin contractility, the formation of actin-based protrusions, and remodeling of cell-cell and cell-matrix adhesions are hallmarks of tumorigenesis and epithelial-to-mesenchymal transition (EMT) [48, 144]. Another cytoskeletal marker of EMT in cancer is the intermediate filament vimentin, which promotes cell stiffening, migration, and loss of E-cadherin at cell-cell junctions [145]. Nakamura and colleagues have used various antibody-conjugated Si nanoneedles operated by AFM to probe the tensile strength of cytoskeletal elements in living cells. High aspect ratio nanoneedles were fabricated by etching AFM tips into 12 μm-long cylinders with diameters of 200 nm and then functionalized with antibodies against the cytoskeletal proteins actin [13] (Fig. 15), tubulin [146], vimentin [44, 147], and nestin [147, 148]. Nanoneedle probes were inserted into cells, allowed to bind targets, and retracted slowly (e.g., 10 μm/s for actin), while the force was measured by AFM cantilever deflection [13]. The pulling forces on the probe

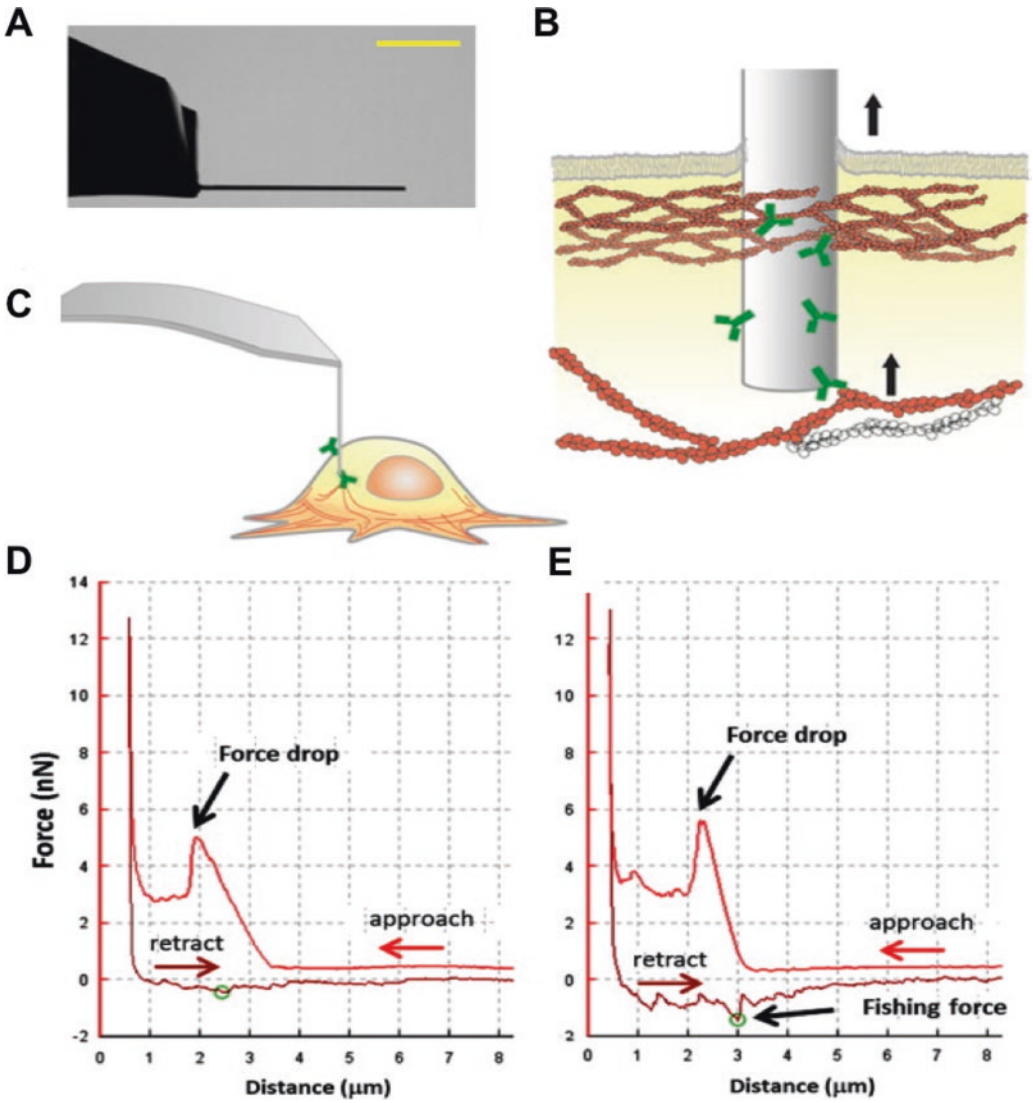

Fig. 15 Antibody-conjugated AFM tips for probing cytoskeletal mechanics. (**a**) Focused ion beam image of nanoneedle etched from an AFM tip. Scale bar = 4 μm. (**b**, **c**) Schematics of antibody-conjugated nanoneedle insertion and binding to actin fibrils. (**d**, **e**) Typical force-distance curves recorded by AFM during approach and retraction of the nanoneedle. The force drop occurs when the nanoneedle initially penetrates the cell membrane. (**d**) Retraction of a nanoneedle with no functionalization results in a smooth force curve. (**e**) Retraction of an anti-actin antibody-conjugated nanoneedle results in a jagged curve and significant "fishing force" peak resulting from antibody-actin unbinding events. (Reproduced with permission from [13]. Copyright 2012, Elsevier)

during the retraction stage, termed "fishing forces," correspond to antibody-target unbinding events (Fig. 15e). Cells could be repeatedly probed (10–20 times) without affecting viability [13, 148]. For anti-actin antibody-conjugated nanoneedles, fishing forces in the 1–2.5 nN range were detected during the retraction stage (twofold higher than observed with nonfunctionalized probes) [13]. Decreased fishing forces, indicative of changes in actin mechanics, induced by treating cells with low doses of cytochalasin D, which depolymerizes F-actin, or Y-27632, which inhibits ROCK-mediated myosin-II activity leading to stress fiber disassembly, were detected by AFM within 5 minutes, before any decrease in actin polymerization could be seen by staining with fluorescent phalloidin. The Nakamura group has also investigated the mechanics of the intermediate filament protein nestin in breast cancer cells. Mouse breast cancer 4T1E cells selected for high metastatic potential had higher fishing forces using anti-nestin conjugated nanoneedles than parental cells, corresponding to higher expression of nestin [148]. Nestin depletion reduced these cells' capacity for directional migration and metastasis [147]. Yamagishi et al. also showed that nestin depletion affected the tensile strength of vimentin, likely via its association with cortical actin, using anti-vimentin functionalized nanoneedles [147].

14 Extraction of Cellular Contents with Nanoneedle Arrays

Antibody-functionalized nanoneedles can also be used to extract proteins from cells. This strategy may be used to perform a spatial biopsy or for immunoprecipitation (IP) or ELISA type assays. Wang et al. used diamond nanoneedle arrays functionalized with protein-binding aptamers to capture and extract cytosolic NF-κB in order to study inflammatory signaling dynamics in cancer cells and neurons [149]. Exposure to double-stranded DNA triggers the degradation of IκB proteins that sequester NF-κB in the cytosol, leading to NF-κB nuclear translocation. The aptamer-conjugated "molecular fishing rods" were interfaced with cells by supergravity, i.e., centrifugation, for 90 seconds and then removed. Temporary disruption of the plasma membrane during this step also allowed for the concurrent delivery of dsDNA into cells. Cells were probed repeatedly following dsDNA exposure for 40 minutes, and captured NF-κB was detected on the nanoneedles by immunofluorescence staining. Fluorescence intensity on the nanoneedles decreased significantly over time in the dsDNA-treated samples but not in controls, indicating (1) that the protein had translocated to the nucleus in response to foreign DNA and (2) that the nanoneedles had penetrated the plasma membrane but not the nucleus. Antibody-functionalized Si nanowire arrays have also been used to capture proteins from living cells [150] (Fig. 16). A human chronic myelogenous leukemia (CML) cell line that grows in suspension and only weakly interacts with Si nanowires was chosen in order to minimize adhesion to the arrays, which were also blocked with polyethylene glycol (PEG) after functionalization. Nanowires functionalized with anti-RFP antibodies were able to pull out the fluorescent protein from transiently transfected cells. Nanowires bearing anti-c-Abl antibodies pulled out endogenous Bcr-Abl fusion proteins, as shown by immunofluorescence staining. Furthermore, anti-Abl conjugated nanowires were positive for Grb-2, which binds to phosphorylated Brc-Abl, indicating that these arrays could be used to co-IP proteins [150] (Fig. 16d).

15 Extraction of Cellular Contents: Hollow Nanostraw Arrays

Arrays of hollow nanoneedles, or nanostraws, were developed by Melosh and colleagues to allow direct fluid access to cell interiors in order to deliver cargos or sample cellular contents [3] (Fig. 5). The Melosh group has reported using aluminum oxide nanostraws to sample intracellular proteins and mRNA from the same cells repeatedly over many hours and

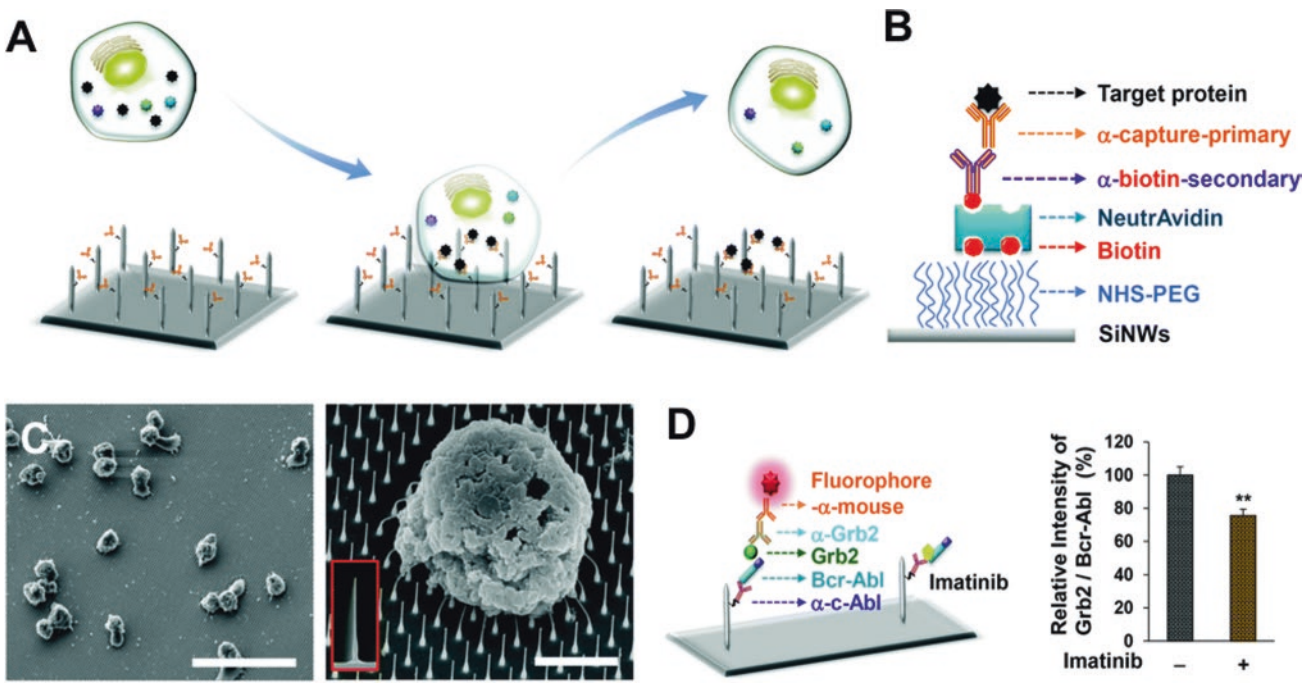

Fig. 16 Silicon nanowire pull-down assay for intracellular sampling. (**a**, **b**) Schematic of the assay. Cells interface transiently with nanowires that are conjugated with biotinylated antibodies for target protein capture. (**c**) SEM images of K562 cells on top of Si nanowires 24 h after plating. Scale bars = 50 μm (left) and 4 μm (right). Inset shows a cross-sectional view of a nanowire at the same scale. (**d**) Co-immunoprecipitation on Si nanowires. Left: schematic of pull-down strategy. Right: intensity of fluorescently labeled secondary antibody relative to negative control (no cell) substrates showing co-IP of Grb2 using anti c-Abl-conjugated nanowires. Data represent mean ± SD ($n = 5$). $^{**}p < 0.01$. (Adapted with permission from [150]. Copyright 2016, Royal Society of Chemistry)

even days in culture with minimal (<5%) cell death [21]. Sampling efficiency was confirmed by measuring fluorescent proteins extracted from GFP-expressing CHO cells. The cells were also transfected with RFP prior to sampling, and extracts showed a gradual increase in red fluorescence over the course of 16 hours. Heat shock protein 27 (HSP27) was also extracted from human iPSC-derived cardiomyocytes over a time course following heat shock. Protein levels were quantified by ELISA and mRNA was measured using qRT-PCR. The levels of protein and mRNA from nanostraw extractions were in good agreement with those from cell lysates and were not present in the absence of electroporation. More recently, Cao et al. reported further optimization of this system for RNA, DNA, and protein delivery [151]. Stamping cells from above with gold nanostraw arrays was also shown to be an efficient means of delivering cargo to adherent cells [152]. This is likely due to the relative speed of insertion compared to cell settling [33, 34, 36]. Magnetic nanoparticles, such as carbon nanotubes, that bind to cytosolic proteins or other molecules can also be loaded into cells and extracted using nanostraws in a magnetic field [153]. Xie and colleagues have also employed hollow nanoneedles with electroporation to repeatedly sample intracellular proteins and deliver cargos [38, 154, 155]. He et al. found that larger alumina nanostraws (450 nm diameter) were able to extract greater quantities of lactate dehydrogenase B (LHDB) from adherent cells, as measured by ELISA [38]. Subsequently, they used a branched nanostraw (BNS) electroporation platform to capture circulating tumor cells (CTC) from a mixed cell suspension, deliver cargos, and extract cytosolic proteins [154] (Fig. 17). MCF7 breast cancer cells were specifically captured by coating nanostraws with antibodies against EpCAM, a CTC marker [156]. The 400-nm-diameter BNS had highly branched surfaces, which facilitated cell capture by greatly increasing surface area (Fig. 17b, c). GFP-encoding plasmid vectors and propidium iodide (which cannot penetrate the intact membrane of living

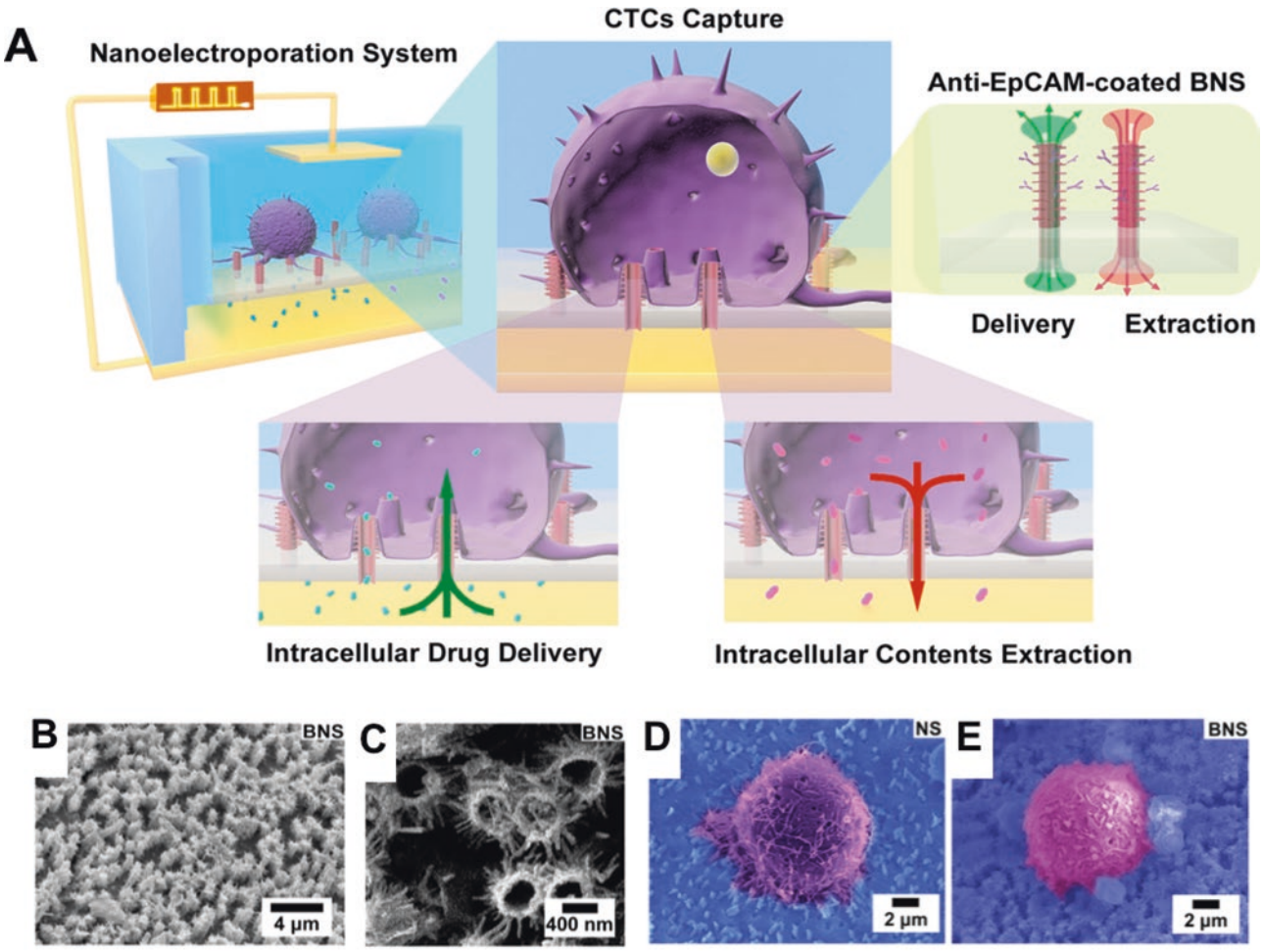

Fig. 17 Multifunctional branched nanostraw-electroporation platform for tumor capture and sampling. (**a**) Schematic of the multifunctional branched nanostraw (BNS) platform. Circulating tumor cells (CTCs) are captured on BNS coated with anti-EpCAM antibody. Captured cells are electroporated to introduce cargo and/or sample cellular contents from the underlying microfluidic channel. (**b**, **c**) SEM images of the branched nanostraw array. (**d**, **e**) Captured MCF7 cells on unbranched (**d**) and branched (**e**) nanostraws. (Adapted with Permission from [154]. Copyright 2019, American Chemical Society)

cells) were delivered to cells following electroporation, and cellular proteins were extracted. Intracellular protein sampling was verified by measuring caspase-3 over time after cells were treated with staurosporine to induce apoptosis. Wen et al. also reported fabrication of nanostraw arrays from Au, Pt, and the conductive polymer poly(3,4)ethylenedioxythiophene (PEDOT) and showed that these could be used for both cargo delivery and protein extraction [155].

16 Extraction of Cellular Contents: Single-Cell Nanobiopsy

Measuring proteins, mRNA, and metabolites in single cells is essential for understanding the heterogeneity of cancer cells. Nanoneedles and nanocapillaries have been used to remove genetic material from individual cells with high spatial precision. In 2007, Uehara et al. used a conventional AFM tip to extract mRNA from different points within rat fibroblasts and confirmed the spatial location of *ACTB* mRNA by fluorescence in situ hybridization (FISH) [104]. Nawarathna and Wickramasinghe also used AFM probes coated with Pt to create a dielectrophoretic force that improved nucleotide capture to profile mRNA extracted from living cells, including breast cancer cells [157, 158]. In both cases, the extracted mRNA was analyzed by qPCR. Pourmand and colleagues used SICM to carefully control nanopipette penetration and extracted the contents of single cells using electrowetting [159] (Fig. 18a–d). The nanocapillary was filled with a hydrophobic liquid whose surface tension changes when a voltage is applied. This change causes the aqueous solution to be drawn into the nanopipette under negative voltage and flow out when the bias is reversed. Extracted mRNA transcripts were analyzed by qRT- PCR. In addition, they extracted individual mitochondria labeled with the vital dye MitoTracker and used next-generation sequencing to sequence the mitochondrial DNA. This method was later used to sample mRNA from cell bodies and neurites of individual neurons to measure the spatial localization of transcripts [160]. Nashimoto et al. used double-barreled nanopipettes guided by SICM to sample mRNA from the nucleus or peripheral cytoplasm of MCF7 cells and quantified the abundance of *GAPDH* and *ACTB* transcripts [161]. Another sampling strategy employed a microfluidic probe (MFP) that can simultaneously inject and aspirate liquid using the principle of hydrodynamic flow confinement [162]. Kashyap et al. used vertically oriented MFPs to locally lyse cancer cell cocultured monolayers and collect DNA/RNA from specific subpopulations, though not from individual cells [162].

Fluidic force microscopy (FluidFM) also uses hollow cantilever AFM tips to dispense or collect picoliter or sub-picoliter volumes of liquid [15] (Fig. 1d). FluidFM nanofluidics in the cantilevers act as pressure-controlled nanopipettes. Guillaume-Gentil et al. found that large proportions of the cytoplasm, up to 4 pl, could be extracted from HeLa cells without causing immediate cell death [163]. This method has been employed by sample intracellular protein from cell nuclei and cytoplasm, and extracted contents have been examined by electron microscopy, enzymatic assays, and qPCR [163].

A variety of nanobiopsy methods have been used to perform metabolomic profiling of single cells. (For a review of single-cell metabolomics, see [164].) Much of the work on single-cell sampling for mass spectroscopy (MS) has been done in plants [165–167], but a number have been performed on mammalian cells. For example, Guillaume-Gentil et al. used FluidFM to sample live cells for MALDI mass spectrometry analysis of metabolites in HeLa cells [168]. Previously, Masujima extracted cellular contents for single-cell MALDI-TOF/MS using nano-electrospray (NES) tips [169]. Aerts et al. used patch clamp pipettes to withdraw up to 2 pl of cytoplasm from rat neurons and observed significant cell-to-cell heterogeneity across 60 analyzed metabolites [170] (Fig. 18e, f). Zhang and Vertes sampled human hepatocarcinoma (HepG2) cells and quantified over 60 metabolites [171]. Mitochondria were also captured from live HepG2 cells using a nano-electrospray tip, and MS analysis revealed unique steroids specific to these organelles [172]. Given the extent of metabolic changes that occur in tumors and tumor stroma, analyzing metabolites on the single cell and population scales will provide valuable information for cancer detection and therapeutics.

17 Future Directions

Nanoneedle probes for intracellular sensing have a great potential to provide insight into cancer dynamics and to expand our ability to detect tumor cells in vivo. Single-cell sampling offers an unprecedented level of spatial resolution and characterization of cell-to-cell heterogeneity. Multiplexed fluorescent and electrochemical reporters mean that dynamic processes can be monitored in real time. As probes grow ever smaller, we are more able to interface with living tissues without cellular destruction. Rapid advances are being made in the use of nanowires and nanoelectrode arrays to probe brains and neuronal cells [173, 174], and these technologies may be adapted for tumor diagnostics or super localized therapeutics. Nano fiber-optics are being developed that can illuminate, irradiate, and manipulate cells with ever-finer spatial resolution [175]. Recently, an ultrasensitive nanomechanical AFM detector comprised of a thin tin dioxide wire coated with PEG and studded with gold nanoparticles was shown to be able to sense forces as low as 160 femtonewtons and acoustic signals down to −30 decibels [176]. In 2019, Jayant et al. reported the use of flexible

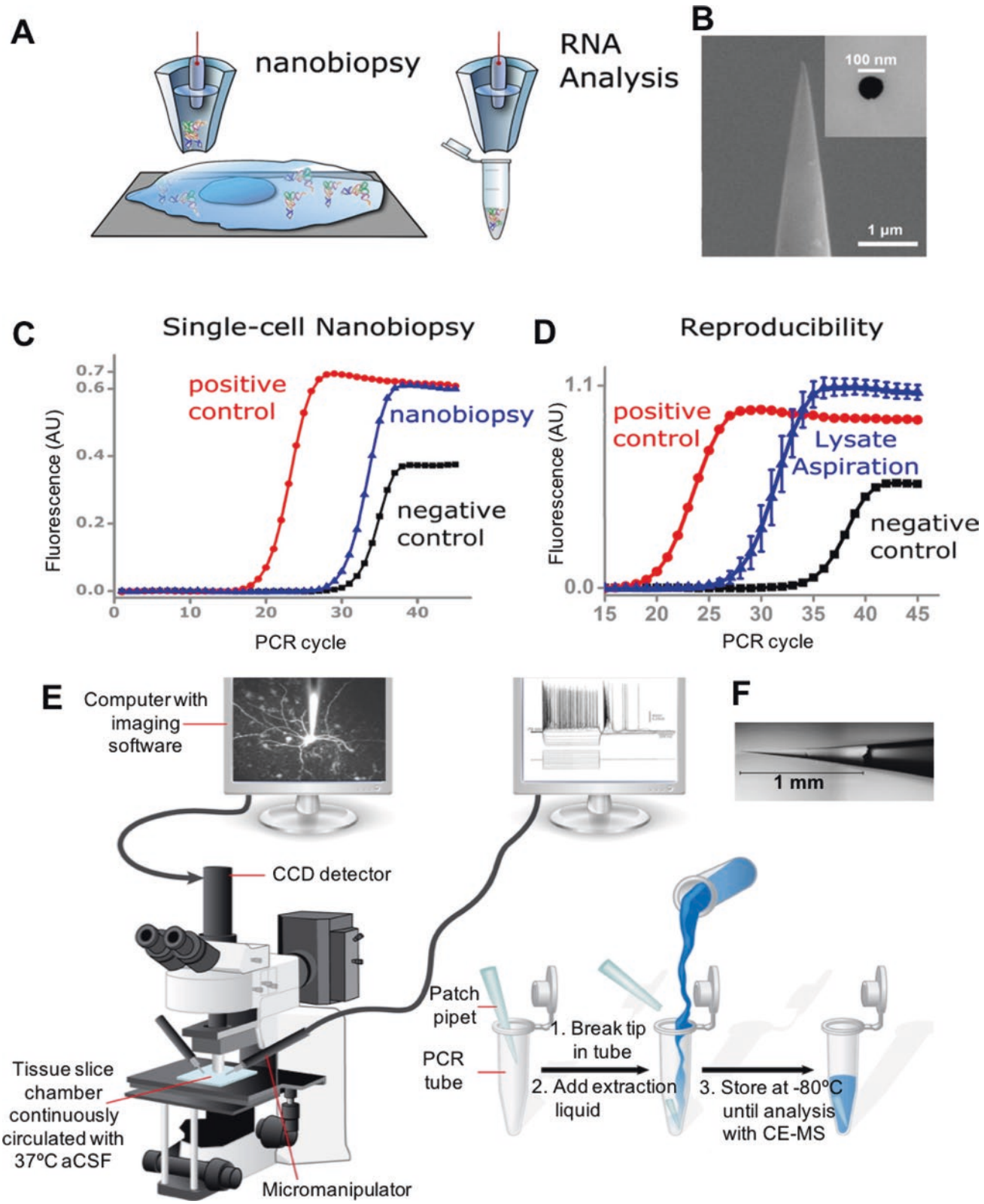

Fig. 18 Extraction of cellular contents for biochemical analysis. (**a**–**d**) Nanobiopsy for mRNA analysis. (**a**) Schematic of nanocapillary needle controlled by SICM to withdraw a small volume of cellular contents. (**b**) SEM of nanocapillary tip (100 nm diameter, inset). (**c**) Post-biopsy qPCR analysis of GFP mRNA from HeLa cells, showing positive control from total cell lysate (~100 cells) in red, negative control (no input) in black, and single-cell nanobiopsy in blue. (**d**) qPCR analysis of four nanobiopsies of the same cell lysate using four different nanoneedles showing good reproducibility. (Adapted with permission from [108]. Copyright 2014, American Chemical Society. **e**–**f**) Patch clamp pipet tip collection of cellular contents for mass spectroscopy. (**e**) Schematic of sample collection. Electrophysiology experiments are conducted on an upright microscope under video observation. Intracellular contents are removed by applying negative pressure. Only cells whose membranes did not rupture during extraction were collected for analysis. Once the patch pipette is removed, the tip is broken off (~1 mm) into a collection tube for MS analysis. (**f**) Photomicrograph of patch tip. (Adapted with permission from [170], https://pubs.acs.org/doi/10.1021/ac500168d. Copyright 2014, American Chemical Society. *Further permissions related to the material excerpted should be directed to the ACS*)

quartz nanopipettes with diameter of 10–25 nm for intracellular electrophysiological recording in the brains of live mice [177]. Another recent innovation was the fabrication of vertical Si nanoneedle arrays on a flexible, transparent elastomer patch which enables direct interfacing with various cell and tissue types as well as real-time imaging [178].

The challenge in the next decade is to bring together this diverse mixture of chemistry, physics, materials science, engineering, and biology to develop platforms that can be readily applied by cancer researchers with clear and targeted readouts. Engineers and cancer researchers will benefit from working together to select from the wide range of nanoneedle innovations those which will provide the most valuable insights into cancer physiology. This can be achieved by clear definitions of biomedical goals (e.g., to build a diagnostic platform that can readily distinguish cancer cells subtypes in vivo or to probe tumor cells to fine-tune personalized medicine) and will be aided by the increasing accessibility of off-the-shelf nanoscale probes for cell biologists and cancer researchers. Most excitingly, there is now substantial evidence that nanoneedle-based approaches can be upscaled using established microfabrication technologies, moving away from the limits of single-cell studies into a regime of network-based analytics and ensemble measurements that can capture the complexity of cancer heterogeneity.

Acknowledgements Thanks to Stuart Higgins (Imperial College, London) for expert advice and invaluable support.

References

1. Chiappini, C., et al. (2015). Biodegradable nanoneedles for localized delivery of nanoparticles in vivo: Exploring the biointerface. *ACS Nano, 9*(5), 5500–5509.
2. Anderson, S. E., & Bau, H. H. (2014). Electrical detection of cellular penetration during microinjection with carbon nanopipettes. *Nanotechnology, 25*(24), 245102.
3. VanDersarl, J. J., Xu, A. M., & Melosh, N. A. (2012). Nanostraws for direct fluidic intracellular access. *Nano Letters, 12*(8), 3881–3886.
4. Vilozny, B., et al. (2011). Reversible cation response with a protein-modified nanopipette. *Analytical Chemistry, 83*(16), 6121–6126.
5. Chiappini, C. (2017). Nanoneedle-based sensing in biological systems. *ACS Sensors, 2*(8), 1086–1102.
6. Bulbul, G., et al. (2018). Nanopipettes as monitoring probes for the single living cell: state of the art and future directions in molecular biology. *Cell, 7*(6), 55.
7. Neves, M., & Martin-Yerga, D. (2018). Advanced nanoscale approaches to single-(bio)entity sensing and imaging. *Biosensors (Basel), 8*(4), 100.
8. McGuire, A. F., Santoro, F., & Cui, B. (2018). Interfacing cells with vertical nanoscale devices: Applications and characterization. *Annual Review of Analytical Chemistry (Palo Alto, California), 11*(1), 101–126.
9. Higgins, S. G., et al. (2020). High-aspect-ratio nanostructured surfaces as biological metamaterials. *Advanced Materials, 32*, e1903862.
10. Chiappini, C., et al. (2015). Mapping local cytosolic enzymatic activity in human esophageal mucosa with porous silicon nanoneedles. *Advanced Materials, 27*(35), 5147–5152.
11. Chiappini, C., et al. (2015). Biodegradable silicon nanoneedles delivering nucleic acids intracellularly induce localized in vivo neovascularization. *Nature Materials, 14*(5), 532–539.
12. Hobbs, R. G., Petkov, N., & Holmes, J. D. (2012). Semiconductor nanowire fabrication by bottom-up and top-down paradigms. *Chemistry of Materials, 24*(11), 1975–1991.
13. Silberberg, Y. R., et al. (2013). Evaluation of the actin cytoskeleton state using an antibody-functionalized nanoneedle and an AFM. *Biosensors & Bioelectronics, 40*(1), 3–9.
14. He, G., et al. (2018). Fabrication of various structures of nanostraw arrays and their applications in gene delivery. *Advanced Materials Interfaces, 5*(10), 1701535.
15. Meister, A., et al. (2009). FluidFM: Combining atomic force microscopy and nanofluidics in a universal liquid delivery system for single cell applications and beyond. *Nano Letters, 9*(6), 2501–2507.
16. Guillaume-Gentil, O., et al. (2014). Force-controlled manipulation of single cells: From AFM to FluidFM. *Trends in Biotechnology, 32*(7), 381–388.
17. van Oorschot, R., et al. (2015). A microfluidic AFM cantilever based dispensing and aspiration platform. *EPJ Techniques and Instrumentation, 2*(1), 4.
18. Singhal, R., et al. (2011). Multifunctional carbon-nanotube cellular endoscopes. *Nature Nanotechnology, 6*(1), 57–64.
19. Shen, M., & Colombo, M. L. (2015). Electrochemical nanoprobes for the chemical detection of neurotransmitters. *Analytical Methods, 7*(17), 7095–7105.
20. Clausmeyer, J., & Schuhmann, W. (2016). Nanoelectrodes: Applications in electrocatalysis, single-cell analysis and high-resolution electrochemical imaging. *Trac-Trends in Analytical Chemistry, 79*, 46–59.
21. Cao, Y., et al. (2017). Nondestructive nanostraw intracellular sampling for longitudinal cell monitoring. *Proceedings of the National Academy of Sciences of the United States of America, 114*(10), E1866–E1874.
22. Hansma, P. K., et al. (1989). The scanning ion-conductance microscope. *Science, 243*(4891), 641–643.
23. Page, A., Perry, D., & Unwin, P. R. (2017). Multifunctional scanning ion conductance microscopy. *Proceedings of the Royal Society A: Mathematical, Physical and Engineering Sciences, 473*(2200), 20160889.
24. Sun, P., Laforge, F. O., & Mirkin, M. V. (2007). Scanning electrochemical microscopy in the 21st century. *Physical Chemistry Chemical Physics, 9*(7), 802–823.
25. Parton, R. G., & Simons, K. (2007). The multiple faces of caveolae. *Nature Reviews. Molecular Cell Biology, 8*(3), 185–194.
26. Wang, Z., et al. (2009). Size and dynamics of caveolae studied using nanoparticles in living endothelial cells. *ACS Nano, 3*(12), 4110–4116.
27. Zhao, W., et al. (2017). Nanoscale manipulation of membrane curvature for probing endocytosis in live cells. *Nature Nanotechnology, 12*(8), 750–756.
28. Gopal, S., et al. (2019). Porous silicon nanoneedles modulate endocytosis to deliver biological payloads. *Advanced Materials, 31*(12), e1806788.
29. Bancelin, S., et al. (2014). Determination of collagen fibril size via absolute measurements of second-harmonic generation signals. *Nature Communications, 5*, 1–8.
30. Maurer, T., et al. (2018). Structural characterization of four different naturally occurring porcine collagen membranes suitable for medical applications. *PLoS One, 13*(10), e0205027.
31. Buch-Manson, N., et al. (2015). Towards a better prediction of cell settling on nanostructure arrays-simple means to complicated ends. *Advanced Functional Materials, 25*(21), 3246–3255.

32. Buch-Manson, N., et al. (2017). Mapping cell behavior across a wide range of vertical silicon nanocolumn densities. *Nanoscale, 9*(17), 5517–5527.
33. Obataya, I., et al. (2005). Mechanical sensing of the penetration of various nanoneedles into a living cell using atomic force microscopy. *Biosensors & Bioelectronics, 20*(8), 1652–1655.
34. Xie, X., et al. (2013). Mechanical model of vertical nanowire cell penetration. *Nano Letters, 13*(12), 6002–6008.
35. Xu, A. M., et al. (2014). Quantification of nanowire penetration into living cells. *Nature Communications, 5*, 3613.
36. Aalipour, A., et al. (2014). Plasma membrane and actin cytoskeleton as synergistic barriers to nanowire cell penetration. *Langmuir, 30*(41), 12362–12367.
37. Xie, X., et al. (2015). Determining the time window for dynamic nanowire cell penetration processes. *ACS Nano, 9*(12), 11667–11677.
38. He, G., et al. (2018). Hollow nanoneedle-electroporation system to extract intracellular protein repetitively and nondestructively. *ACS Sensors, 3*(9), 1675–1682.
39. Dipalo, M., et al. (2018). Cells adhering to 3D vertical nanostructures: Cell membrane reshaping without stable internalization. *Nano Letters, 18*(9), 6100–6105.
40. Duan, X., et al. (2011). Intracellular recordings of action potentials by an extracellular nanoscale field-effect transistor. *Nature Nanotechnology, 7*(3), 174–179.
41. Angle, M. R., et al. (2014). Penetration of cell membranes and synthetic lipid bilayers by nanoprobes. *Biophysical Journal, 107*(9), 2091–2100.
42. Lee, J. H., et al. (2016). Spontaneous internalization of cell penetrating peptide-modified nanowires into primary neurons. *Nano Letters, 16*(2), 1509–1513.
43. Han, S. W., et al. (2005). Gene expression using an ultrathin needle enabling accurate displacement and low invasiveness. *Biochemical and Biophysical Research Communications, 332*(3), 633–639.
44. Kawamura, R., et al. (2016). High efficiency penetration of antibody-immobilized nanoneedle thorough plasma membrane for in situ detection of cytoskeletal proteins in living cells. *Journal of Nanobiotechnology, 14*(1), 74.
45. Simonis, M., et al. (2017). Survival rate of eukaryotic cells following electrophoretic nanoinjection. *Scientific Reports, 7*, 41277.
46. Zhou, J., et al. (2018). The effects of surface topography of nanostructure arrays on cell adhesion. *Physical Chemistry Chemical Physics, 20*(35), 22946–22951.
47. Swaminathan, V., et al. (2011). Mechanical stiffness grades metastatic potential in patient tumor cells and in cancer cell lines. *Cancer Research, 71*(15), 5075–5080.
48. Cross, S. E., et al. (2007). Nanomechanical analysis of cells from cancer patients. *Nature Nanotechnology, 2*(12), 780–783.
49. Handel, C., et al. (2015). Cell membrane softening in human breast and cervical cancer cells. *New Journal of Physics, 17*, 083008.
50. Anderson, S. E., & Bau, H. H. (2015). Carbon nanoelectrodes for single-cell probing. *Nanotechnology, 26*(18), 185101.
51. Novak, P., et al. (2009). Nanoscale live-cell imaging using hopping probe ion conductance microscopy. *Nature Methods, 6*(4), 279–281.
52. Yum, K., et al. (2009). Mechanochemical delivery and dynamic tracking of fluorescent quantum dots in the cytoplasm and nucleus of living cells. *Nano Letters, 9*(5), 2193–2198.
53. Shalek, A. K., et al. (2010). Vertical silicon nanowires as a universal platform for delivering biomolecules into living cells. *Proceedings of the National Academy of Sciences of the United States of America, 107*(5), 1870–1875.
54. Chen, X., et al. (2007). A cell nanoinjector based on carbon nanotubes. *Proceedings of the National Academy of Sciences of the United States of America, 104*(20), 8218–8222.
55. Adam Seger, R., et al. (2012). Voltage controlled nano-injection system for single-cell surgery. *Nanoscale, 4*(19), 5843–5846.
56. Peer, E., et al. (2012). Hollow nanoneedle array and its utilization for repeated administration of biomolecules to the same cells. *ACS Nano, 6*(6), 4940–4946.
57. Loh, O., et al. (2009). Nanofountain-probe-based high-resolution patterning and single-cell injection of functionalized nanodiamonds. *Small, 5*(14), 1667–1674.
58. Ying, Y. L., et al. (2017). Advanced electroanalytical chemistry at nanoelectrodes. *Chemical Science, 8*(5), 3338–3348.
59. Hennig, S., et al. (2015). Instant live-cell super-resolution imaging of cellular structures by nanoinjection of fluorescent probes. *Nano Letters, 15*(2), 1374–1381.
60. Yang, R., et al. (2018). Monoclonal cell line generation and CRISPR/Cas9 manipulation via single-cell electroporation. *Small, 14*(12), e1702495.
61. Kang, W., et al. (2013). Nanofountain probe electroporation (NFP-E) of single cells. *Nano Letters, 13*(6), 2448–2457.
62. Giraldo-Vela, J. P., et al. (2015). Single-cell detection of mRNA expression using nanofountain-probe electroporated molecular beacons. *Small, 11*(20), 2386–2391.
63. Tan, W., Wang, K., & Drake, T. J. (2004). Molecular beacons. *Current Opinion in Chemical Biology, 8*(5), 547–553.
64. Mereiter, S., et al. (2019). Glycosylation in the era of cancer-targeted therapy: Where are we heading? *Cancer Cell, 36*(1), 6–16.
65. Xie, X., et al. (2013). Nanostraw-electroporation system for highly efficient intracellular delivery and transfection. *ACS Nano, 7*(5), 4351–4358.
66. Caprettini, V., et al. (2017). Soft electroporation for delivering molecules into tightly adherent mammalian cells through 3D hollow nanoelectrodes. *Scientific Reports, 7*(1), 8524.
67. Xu, A. M., et al. (2017). Direct intracellular delivery of cell-impermeable probes of protein glycosylation by using nanostraws. *Chembiochem, 18*(7), 623–628.
68. Shen, X., et al. (2019). Biodegradable nanosyringes for intracellular amplification-based dual-diagnosis and gene therapy in single living cells. *Chemical Science, 10*(24), 6113–6119.
69. Hansel, C. S., et al. (2019). Nanoneedle-mediated stimulation of cell mechanotransduction machinery. *ACS Nano, 13*(3), 2913–2926.
70. Pandey, S., et al. (2013). Gold nanorods mediated controlled release of doxorubicin: Nano-needles for efficient drug delivery. *Journal of Materials Science. Materials in Medicine, 24*(7), 1671–1681.
71. Pan, W., et al. (2013). Multiplexed detection and imaging of intracellular mRNAs using a four-color nanoprobe. *Analytical Chemistry, 85*(21), 10581–10588.
72. Pan, W., et al. (2015). Simultaneous visualization of multiple mRNAs and matrix metalloproteinases in living cells using a fluorescence nanoprobe. *Chemistry, 21*(16), 6070–6073.
73. Hong, Y., et al. (2014). Molecular recognition of proteolytic activity in metastatic cancer cells using fluorogenic gold nanoprobes. *Biosensors & Bioelectronics, 57*, 171–178.
74. Lee, H., & Kim, Y. P. (2015). Fluorescent and bioluminescent nanoprobes for in vitro and in vivo detection of matrix metalloproteinase activity. *BMB Reports, 48*(6), 313–318.
75. Sun, L., et al. (2018). MMP-2-responsive fluorescent nanoprobes for enhanced selectivity of tumor cell uptake and imaging. *Biomaterials Science, 6*(10), 2619–2626.
76. Zhan, R., et al. (2020). An Au-Se nanoprobe for the evaluation of the invasive potential of breast cancer cells via imaging the sequential activation of uPA and MMP-2. *Analyst, 145*(3), 1008–1013.
77. Tavallaie, R., et al. (2018). Nucleic acid hybridization on an electrically reconfigurable network of gold-coated magnetic nanoparticles enables microRNA detection in blood. *Nature Nanotechnology, 13*(11), 1066–1071.
78. Li, C., et al. (2020). Intracellular sensors based on carbonaceous nanomaterials: A review. *Journal of the Electrochemical Society, 167*(3), 037540.

79. Navas-Moreno, M., et al. (2017). Nanoparticles for live cell microscopy: A surface-enhanced Raman scattering perspective. *Scientific Reports, 7*(1), 4471.
80. Bruzas, I., et al. (2018). Advances in surface-enhanced Raman spectroscopy (SERS) substrates for lipid and protein characterization: Sensing and beyond. *Analyst, 143*(17), 3990–4008.
81. Szekeres, G. P., & Kneipp, J. (2019). SERS probing of proteins in gold nanoparticle agglomerates. *Frontiers in Chemistry, 7*, 30.
82. Hanif, S., et al. (2017). Organic cyanide decorated SERS active nanopipettes for quantitative detection of hemeproteins and Fe(3+) in single cells. *Analytical Chemistry, 89*(4), 2522–2530.
83. Huang, J. A., et al. (2019). On-demand intracellular delivery of single particles in single cells by 3D hollow nanoelectrodes. *Nano Letters, 19*(2), 722–731.
84. Nguyen, T. D., et al. (2019). Nanostars on nanopipette tips: A Raman probe for quantifying oxygen levels in hypoxic single cells and tumours. *Angewandte Chemie (International Ed. in English), 58*(9), 2710–2714.
85. Yum, K., et al. (2011). Biofunctionalized nanoneedles for the direct and site-selective delivery of probes into living cells. *Biochimica et Biophysica Acta, 1810*(3), 330–338.
86. Kihara, T., et al. (2009). Development of a method to evaluate caspase-3 activity in a single cell using a nanoneedle and a fluorescent probe. *Biosensors & Bioelectronics, 25*(1), 22–27.
87. Na, Y. R., et al. (2013). Probing enzymatic activity inside living cells using a nanowire-cell "sandwich" assay. *Nano Letters, 13*(1), 153–158.
88. Kihara, T., et al. (2010). Development of a novel method to detect intrinsic mRNA in a living cell by using a molecular beacon-immobilized nanoneedle. *Biosensors & Bioelectronics, 26*(4), 1449–1454.
89. Matsumoto, D., et al. (2015). Oscillating high-aspect-ratio monolithic silicon nanoneedle array enables efficient delivery of functional bio-macromolecules into living cells. *Scientific Reports, 5*, 15325.
90. White, K. A., Grillo-Hill, B. K., & Barber, D. L. (2017). Cancer cell behaviors mediated by dysregulated pH dynamics at a glance. *Journal of Cell Science, 130*(4), 663–669.
91. Szpaderska, A. M., & Frankfater, A. (2001). An intracellular form of cathepsin B contributes to invasiveness in cancer. *Cancer Research, 61*(8), 3493–3500.
92. Swisher, L. Z., et al. (2015). Quantitative electrochemical detection of cathepsin B activity in breast cancer cell lysates using carbon nanofiber nanoelectrode arrays toward identification of cancer formation. *Nanomedicine, 11*(7), 1695–1704.
93. DeBerardinis, R. J., & Chandel, N. S. (2016). Fundamentals of cancer metabolism. *Science Advances, 2*(5), e1600200.
94. Lin, T. E., et al. (2018). Electrochemical imaging of cells and tissues. *Chemical Science, 9*(20), 4546–4554.
95. Fan, Y., Han, C., & Zhang, B. (2016). Recent advances in the development and application of nanoelectrodes. *Analyst, 141*(19), 5474–5487.
96. Pan, R., et al. (2016). Nanokit for single-cell electrochemical analyses. *Proceedings of the National Academy of Sciences of the United States of America, 113*(41), 11436–11440.
97. Pan, R., & Jiang, D. (2019). Nanokits for the electrochemical quantification of enzyme activity in single living cells. *Methods in Enzymology, 628*, 173–189.
98. Xu, H., et al. (2019). Phosphate assay kit in one cell for electrochemical detection of intracellular phosphate ions at single cells. *Frontiers in Chemistry, 7*, 360.
99. Qian, R. C., Lv, J., & Long, Y. T. (2018). Ultrafast mapping of subcellular domains via nanopipette-based electroosmotically modulated delivery into a single living cell. *Analytical Chemistry, 90*(22), 13744–13750.
100. Pernicova, I., & Korbonits, M. (2014). Metformin--mode of action and clinical implications for diabetes and cancer. *Nature Reviews. Endocrinology, 10*(3), 143–156.
101. Ozel, R. E., et al. (2015). Single-cell intracellular nano-pH probes. *RSC Advances, 5*(65), 52436–52443.
102. Lee, H. S., et al. (2012). Reversible swelling of chitosan and quaternary ammonium modified chitosan brush layers: Effect of pH and counter anion size and functionality. *Journal of Materials Chemistry, 22*(37), 19605–19616.
103. Cervera, J., et al. (2006). Ionic conduction, rectification, and selectivity in single conical nanopores. *The Journal of Chemical Physics, 124*(10), 104706.
104. Umehara, S., et al. (2009). Label-free biosensing with functionalized nanopipette probes. *Proceedings of the National Academy of Sciences of the United States of America, 106*(12), 4611–4616.
105. Nascimento, R. A., et al. (2016). Single cell "glucose nanosensor" verifies elevated glucose levels in individual cancer cells. *Nano Letters, 16*(2), 1194–1200.
106. Liberti, M. V., & Locasale, J. W. (2016). The Warburg effect: How does it benefit cancer cells? *Trends in Biochemical Sciences, 41*(3), 211–218.
107. Smith, S. K., et al. (2018). Carbon-fiber microbiosensor for monitoring rapid lactate fluctuations in brain tissue using fast-scan cyclic voltammetry. *Analytical Chemistry, 90*(21), 12994–12999.
108. Actis, P., et al. (2014). Electrochemical nanoprobes for single-cell analysis. *ACS Nano, 8*(1), 875–884.
109. Zhang, Y., et al. (2016). Spearhead nanometric field-effect transistor sensors for single-cell analysis. *ACS Nano, 10*(3), 3214–3221.
110. Ying, Y. L., et al. (2018). Asymmetric nanopore electrode-based amplification for electron transfer imaging in live cells. *Journal of the American Chemical Society, 140*(16), 5385–5392.
111. Huang, F., et al. (2018). Photoactivated specific mRNA detection in single living cells by coupling "signal-on" fluorescence and "signal-off" electrochemical signals. *Nano Letters, 18*(8), 5116–5123.
112. Dhar, S. K., et al. (2011). Manganese superoxide dismutase is a p53-regulated gene that switches cancers between early and advanced stages. *Cancer Research, 71*(21), 6684–6695.
113. Moloney, J. N., & Cotter, T. G. (2018). ROS signalling in the biology of cancer. *Seminars in Cell & Developmental Biology, 80*, 50–64.
114. Wang, K., et al. (2019). Targeting metabolic-redox circuits for cancer therapy. *Trends in Biochemical Sciences, 44*(5), 401–414.
115. Arbault, S., et al. (1995). Monitoring an oxidative stress mechanism at a single human fibroblast. *Analytical Chemistry, 67*(19), 3382–3390.
116. Sun, P., et al. (2008). Nanoelectrochemistry of mammalian cells. *Proceedings of the National Academy of Sciences of the United States of America, 105*(2), 443–448.
117. Ozel, R. E., et al. (2018). Functionalized quartz nanopipette for intracellular superoxide sensing: A tool for monitoring reactive oxygen species levels in single living cell. *ACS Sensors, 3*(7), 1316–1321.
118. Zhang, Y., et al. (2013). ROS play a critical role in the differentiation of alternatively activated macrophages and the occurrence of tumor-associated macrophages. *Cell Research, 23*(7), 898–914.
119. Wang, Y., et al. (2012). Nanoelectrodes for determination of reactive oxygen and nitrogen species inside murine macrophages. *Proceedings of the National Academy of Sciences of the United States of America, 109*(29), 11534–11539.
120. Marquitan, M., et al. (2016). Intracellular hydrogen peroxide detection with functionalised nanoelectrodes. *ChemElectroChem, 3*(12), 2125–2129.
121. Rawson, F. J., et al. (2015). Fast, ultrasensitive detection of reactive oxygen species using a carbon nanotube based-electrocatalytic intracellular sensor. *ACS Applied Materials & Interfaces, 7*(42), 23527–23537.
122. Ding, S., et al. (2020). Sensitive and selective measurement of hydroxyl radicals at subcellular level with tungsten nanoelectrodes. *Analytical Chemistry, 92*(3), 2543–2549.

123. Zhang, X. W., et al. (2017). Real-time intracellular measurements of ROS and RNS in living cells with single core-shell nanowire electrodes. *Angewandte Chemie (International Ed. in English), 56*(42), 12997–13000.
124. Hu, K., et al. (2019). Electrochemical measurements of reactive oxygen and nitrogen species inside single phagolysosomes of living macrophages. *Journal of the American Chemical Society, 141*(11), 4564–4568.
125. Li, X., et al. (2015). Quantitative measurement of transmitters in individual vesicles in the cytoplasm of single cells with nanotip electrodes. *Angewandte Chemie (International Ed. in English), 54*(41), 11978–11982.
126. Li, Y., et al. (2017). Direct electrochemical measurements of reactive oxygen and nitrogen species in nontransformed and metastatic human breast cells. *Journal of the American Chemical Society, 139*(37), 13055–13062.
127. Clapham, D. E. (2007). Calcium signaling. *Cell, 131*(6), 1047–1058.
128. Son, D., et al. (2011). Nanoneedle transistor-based sensors for the selective detection of intracellular calcium ions. *ACS Nano, 5*(5), 3888–3895.
129. Petronek, M. S., et al. (2019). Linking cancer metabolic dysfunction and genetic instability through the lens of iron metabolism. *Cancers (Basel), 11*(8), 1077.
130. Bulbul, G., et al. (2019). Employment of iron-binding protein from Haemophilus influenzae in functional nanopipettes for iron monitoring. *ACS Chemical Neuroscience, 10*(4), 1970–1977.
131. Kim, H. S., Kim, Y. J., & Seo, Y. R. (2015). An overview of carcinogenic heavy metal: Molecular toxicity mechanism and prevention. *Journal of Cancer Prevention, 20*(4), 232–240.
132. Leyssens, L., et al. (2017). Cobalt toxicity in humans-A review of the potential sources and systemic health effects. *Toxicology, 387*, 43–56.
133. Actis, P., et al. (2011). Voltage-controlled metal binding on polyelectrolyte-functionalized nanopores. *Langmuir, 27*(10), 6528–6533.
134. Actis, P., et al. (2012). Copper sensing with a prion protein modified nanopipette. *RSC Advances, 2*(31), 11638–11640.
135. Sa, N., Fu, Y., & Baker, L. A. (2010). Reversible cobalt ion binding to imidazole-modified nanopipettes. *Analytical Chemistry, 82*(24), 9963–9966.
136. Miao, R., et al. (2014). Silicon nanowire-based fluorescent nanosensor for complexed Cu2+ and its bioapplications. *Nano Letters, 14*(6), 3124–3129.
137. Abbott, J., et al. (2020). A nanoelectrode array for obtaining intracellular recordings from thousands of connected neurons. *Nature Biomedical Engineering, 4*(2), 232–241.
138. Abbott, J., et al. (2017). CMOS nanoelectrode array for all-electrical intracellular electrophysiological imaging. *Nature Nanotechnology, 12*(5), 460–466.
139. Robinson, J. T., et al. (2012). Vertical nanowire electrode arrays as a scalable platform for intracellular interfacing to neuronal circuits. *Nature Nanotechnology, 7*(3), 180–184.
140. Xie, C., et al. (2012). Intracellular recording of action potentials by nanopillar electroporation. *Nature Nanotechnology, 7*(3), 185–190.
141. Lin, Z. C., et al. (2017). Accurate nanoelectrode recording of human pluripotent stem cell-derived cardiomyocytes for assaying drugs and modeling disease. *Microsystems & Nanoengineering, 3*, 16080.
142. Staufer, O., et al. (2019). Adhesion stabilized en masse intracellular electrical recordings from multicellular assemblies. *Nano Letters, 19*(5), 3244–3255.
143. Caprettini, V., et al. (2018). Enhanced Raman investigation of cell membrane and intracellular compounds by 3D plasmonic nanoelectrode arrays. *Advanced Science (Weinheim), 5*(12), 1800560.
144. Deville, S. S., & Cordes, N. (2019). The extracellular, cellular, and nuclear stiffness, a trinity in the cancer resistome-a review. *Frontiers in Oncology, 9*, 1376.
145. Liu, C. Y., et al. (2015). Vimentin contributes to epithelial-mesenchymal transition cancer cell mechanics by mediating cytoskeletal organization and focal adhesion maturation. *Oncotarget, 6*(18), 15966–15983.
146. Silberberg, Y. R., et al. (2014). Detection of microtubules in vivo using antibody-immobilized nanoneedles. *Journal of Bioscience and Bioengineering, 117*(1), 107–112.
147. Yamagishi, A., et al. (2019). The structural function of nestin in cell body softening is correlated with cancer cell metastasis. *International Journal of Biological Sciences, 15*(7), 1546–1556.
148. Mieda, S., et al. (2012). Mechanical force-based probing of intracellular proteins from living cells using antibody-immobilized nanoneedles. *Biosensors & Bioelectronics, 31*(1), 323–329.
149. Wang, Z. X., et al. (2015). Interrogation of cellular innate immunity by diamond-nanoneedle-assisted intracellular molecular fishing. *Nano Letters, 15*(10), 7058–7063.
150. Choi, S., et al. (2016). Probing protein complexes inside living cells using a silicon nanowire-based pull-down assay. *Nanoscale, 8*(22), 11380–11384.
151. Cao, Y., et al. (2018). Universal intracellular biomolecule delivery with precise dosage control. *Science Advances, 4*(10), eaat8131.
152. Zhang, B., et al. (2019). Nanostraw membrane stamping for direct delivery of molecules into adhesive cells. *Scientific Reports, 9*(1), 6806.
153. Yang, Z., et al. (2014). Molecular extraction in single live cells by sneaking in and out magnetic nanomaterials. *Proceedings of the National Academy of Sciences of the United States of America, 111*(30), 10966–10971.
154. He, G., et al. (2019). Multifunctional branched nanostraw-electroporation platform for intracellular regulation and monitoring of circulating tumor cells. *Nano Letters, 19*(10), 7201–7209.
155. Wen, R., et al. (2019). Intracellular delivery and sensing system based on electroplated conductive nanostraw arrays. *ACS Applied Materials & Interfaces, 11*(47), 43936–43948.
156. Munz, M., Baeuerle, P. A., & Gires, O. (2009). The emerging role of EpCAM in cancer and stem cell signaling. *Cancer Research, 69*(14), 5627–5629.
157. Nawarathna, D., et al. (2011). Targeted messenger RNA profiling of transfected breast cancer gene in a living cell. *Analytical Biochemistry, 408*(2), 342–344.
158. Nawarathna, D., Turan, T., & Wickramasinghe, H. K. (2009). Selective probing of mRNA expression levels within a living cell. *Applied Physics Letters, 95*(8), 83117.
159. Actis, P., et al. (2014). Compartmental genomics in living cells revealed by single-cell nanobiopsy. *ACS Nano, 8*(1), 546–553.
160. Toth, E. N., et al. (2018). Single-cell nanobiopsy reveals compartmentalization of mRNAs within neuronal cells. *The Journal of Biological Chemistry, 293*(13), 4940–4951.
161. Nashimoto, Y., et al. (2016). Evaluation of mRNA localization using double barrel scanning ion conductance microscopy. *ACS Nano, 10*(7), 6915–6922.
162. Kashyap, A., et al. (2016). Selective local lysis and sampling of live cells for nucleic acid analysis using a microfluidic probe. *Scientific Reports, 6*, 29579.
163. Guillaume-Gentil, O., et al. (2016). Tunable single-cell extraction for molecular analyses. *Cell, 166*(2), 506–516.
164. Duncan, K. D., Fyrestam, J., & Lanekoff, I. (2019). Advances in mass spectrometry based single-cell metabolomics. *Analyst, 144*(3), 782–793.
165. Gong, X., et al. (2014). Single cell analysis with probe ESI-mass spectrometry: Detection of metabolites at cellular and subcellular levels. *Analytical Chemistry, 86*(8), 3809–3816.

166. Yin, R., Prabhakaran, V., & Laskin, J. (2018). Quantitative extraction and mass spectrometry analysis at a single-cell level. *Analytical Chemistry, 90*(13), 7937–7945.
167. Yin, R., Prabhakaran, V., & Laskin, J. (2019). Electroosmotic extraction coupled to mass spectrometry analysis of metabolites in live cells. *Methods in Enzymology, 628*, 293–307.
168. Guillaume-Gentil, O., et al. (2017). Single-cell mass spectrometry of metabolites extracted from live cells by fluidic force microscopy. *Analytical Chemistry, 89*(9), 5017–5023.
169. Masujima, T. (2009). Live single-cell mass spectrometry. *Analytical Sciences, 25*(8), 953–960.
170. Aerts, J. T., et al. (2014). Patch clamp electrophysiology and capillary electrophoresis-mass spectrometry metabolomics for single cell characterization. *Analytical Chemistry, 86*(6), 3203–3208.
171. Zhang, L., & Vertes, A. (2015). Energy charge, redox state, and metabolite turnover in single human hepatocytes revealed by capillary microsampling mass spectrometry. *Analytical Chemistry, 87*(20), 10397–10405.
172. Esaki, T., & Masujima, T. (2015). Fluorescence probing live single-cell mass spectrometry for direct analysis of organelle metabolism. *Analytical Sciences, 31*(12), 1211–1213.
173. Zhao, Y. L., et al. (2019). Scalable ultrasmall three-dimensional nanowire transistor probes for intracellular recording. *Nature Nanotechnology, 14*(8), 783–790.
174. Tullii, G., et al. (2019). High-aspect-ratio semiconducting polymer pillars for 3D cell cultures. *ACS Applied Materials & Interfaces, 11*(31), 28125–28137.
175. Li, Y. C., Liu, X. S., & Li, B. J. (2019). Single-cell biomagnifier for optical nanoscopes and nanotweezers. *Light-Science & Applications, 8*, 1–12.
176. Huang, Q., et al. (2017). Nanofibre optic force transducers with sub-piconewton resolution via near-field plasmon-dielectric interactions. *Nature Photonics, 11*(6), 352–355.
177. Jayant, K., et al. (2019). Flexible nanopipettes for minimally invasive intracellular electrophysiology in vivo. *Cell Reports, 26*(1), 266–278 e5.
178. Kim, H., et al. (2018). Flexible elastomer patch with vertical silicon nanoneedles for intracellular and intratissue nanoinjection of biomolecules. *Science Advances, 4*(11), eaau6972.
179. Kim, W., et al. (2007). Interfacing silicon nanowires with mammalian cells. *Journal of the American Chemical Society, 129*(23), 7228–7229.